Optimizing IFN alpha therapy against Myeloproliferative Neoplasms

Gurvan Hermange[1], Paul-Henry Cournède[1*], and Isabelle Plo[2, 3, 4*]

[1]Université Paris-Saclay, CentraleSupélec, Laboratory of Mathematics and Informatics (MICS), Gif-sur-Yvette, France.
[2]INSERM U1287 (INSERM, Gustave Roussy, Université Paris-Saclay), Villejuif, France
[3]Gustave Roussy, Villejuif, France
[4]Université Paris-Saclay, Villejuif, France
[*]corresponding authors: paul-henry.cournede@centralesupelec.fr ; isabelle.plo@gustaveroussy.fr

Supplemental Materials and Methods

We present the data used in this work in section A, and our model in section B. Section C presents the parameter estimation procedure that allows us to make long-term predictions of the effect of IFNα therapy against MPN. In § C.1, we present how the hierarchical Bayesian estimation is performed, and in § C.2, how we estimate the parameters for a new patient.
In section D, we describe how we model the expansion of the $JAK2^{V617F}$ heterozygous and homozygous mutated clones in the absence of IFNα, and then, the criterion for deciding at which age the therapy could be interrupted.
In sections E and F, we detail the methods used for optimizing the therapy and the experimental design, respectively.
The detail of our results is presented in section G. In § G.1, we detail the results of the prediction; in § G.2, those for the optimization; and in § G.3, those for the experimental design.

Contents

A Data and observation model

The data we use in this study come from [15]. In particular, we consider the 19 $JAK2^{V617F}$ MPN patients studied in [9]. Observations originally consisted of the clonal architecture measurements of progenitors and the proportion of mutated alleles (VAF - Variant Allele Frequency) in mature cells. We denote by $\mathcal{D} = \{\mathcal{D}_i\}_{i\in\{1,\cdots,N\}}$ the dataset for all $N = 19$ patients. For a patient i, the data consist of observations at different times $t_k^{(i)}$ from the beginning of the therapy ($t = 0$). The VAF $\hat{y}_k^{(i)}$ is measured in peripheral blood, that is, among mature cells. Such a measurement can easily be obtained in clinical routine. We consider that the measurements are noisy, and use the same observation model as Mosca et al. [15]. For mature cells, it is assumed a Gaussian noise with a variance that depends on the true VAF $y_k^{(i)} \in [0, 1]$ at time $t_k^{(i)}$:

$$\hat{y}_k^{(i)} \mid y_k^{(i)} \sim \mathcal{N}\left(y_k^{(i)}, y_k^{(i)}\left(1 - y_k^{(i)}\right)\sigma_m^2\right) \tag{A.1}$$

with σ_m to be estimated.

The clonal architecture of purified $CD34^+$ progenitors is measured at different time points. To determine this clonal architecture from a blood sample, several experimental steps are required, as presented in [15]. Such measurements cannot be easily obtained in clinical routine, especially not every three or four months. When measuring the clonal architecture at time $t_k^{(i)}$, we get $\hat{n}_{k,wt}^{(i)}$, $\hat{n}_{k,het}^{(i)}$, and $\hat{n}_{k,hom}^{(i)}$ of wt (wild-type), heterozygous (het) and homozygous (hom) mutated progenitor cells, respectively. From these values, we can compute the mutated heterozygous Clonal Fraction (CF):

$$\hat{z}_{k,het}^{(i)} = \frac{\hat{n}_{k,het}^{(i)}}{\hat{n}_{k,wt}^{(i)} + \hat{n}_{k,het}^{(i)} + \hat{n}_{k,hom}^{(i)}}$$

as well as the mutated homozygous CF:

$$\hat{z}_{k,hom}^{(i)} = \frac{\hat{n}_{k,hom}^{(i)}}{\hat{n}_{k,wt}^{(i)} + \hat{n}_{k,het}^{(i)} + \hat{n}_{k,hom}^{(i)}}$$

The uncertainty associated with the measured CF comes from the fact that only a limited number of progenitor cells are sampled. Following what was done in Mosca et al. [15] (and also in [1]), we consider that the observed immature cells are randomly sampled from an unknown but very large set of immature cells so that the uncertainty might be modeled by a multinomial distribution:

$$\mathbb{P}\left[\hat{n}_{k,hom}^{(i)} = n_1, \hat{n}_{k,het}^{(i)} = n_2, \hat{n}_{k,hom}^{(i)} = n_3 \mid z_{k,het}, z_{k,hom}\right] = \frac{(n_1 + n_2 + n_3)!}{n_1!n_2!n_3!} z_{k,wt}^{n_1} z_{k,het}^{n_2} z_{k,hom}^{n_3}$$

where $z_{k,wt}$, $z_{k,het}$, and $z_{k,hom}$ are the true CF for wt, het, and hom progenitor cells, respectively (with $z_{k,wt} = 1 - z_{k,het} - z_{k,hom}$).

Both the CF and the VAF are ratios whose values range between 0 and 1. The CF refers to a ratio of mutated cells, while the VAF refers to a ratio of mutated alleles. Implicitly, the VAF and the CF refer to mature and progenitor cells, respectively. We will explicitly specify when the VAF and the CF refer to the HSCs.

Finally, $\mathcal{I}^{(i)}$ corresponds to the set of observation times for patient i, and we have:

$$\mathcal{D}^{(i)} = \left(t_k^{(i)}, \hat{n}_{k,wt}^{(i)}, \hat{n}_{k,het}^{(i)}, \hat{n}_{k,hom}^{(i)}, \hat{y}_k^{(i)}\right)_{k\in\mathcal{I}^{(i)}}$$

Clinical and experimental data for each of the 19 $JAK2^{V617F}$ MPN patients are represented in Figures A.1 to A.19. The patients' ids are those used by Mosca et al. [15]. In this article, we will focus on the three patients presented in Tab. A.1. These are the patients that will be excluded from the cohort of the 19 patients, each in turn, such that we could study for them:

- our capacity to predict their long-term responses to IFNα,

	#12	#18	#32
Age at t_0 [years]	63	57	52
Disease	PV	PMF	PV
Sex	F	F	M

Table A.1: List of the patients we focus on in this study. For each of them, we indicate their age at the beginning of the therapy (t_0), their disease (PV: polycythemia vera; PMF: primary myelofibrosis), and whether they are a female (F) or a male (M). The patients' numbers are the same as in the article of Mosca et al. [15]. More information about the patients can be found in their study.

- how to optimize their therapy,
- and what would have been the optimal experimental design.

Suppose we consider, for example, patient #32. When we focus on this patient, we exclude them from the cohort. Thus, we also do not consider all of their CF measurements, but only two of them: one at the diagnostic time and one later. We exclude the other CF observations to mimic the fact that this patient would be observed following a realistic clinical routine. The excluded data will be used to assess the quality of the predictions. However, when we focus on another patient, for example, patient #12, then patient #32 is part of the cohort. In this case, we consider all the observations for patient #32.

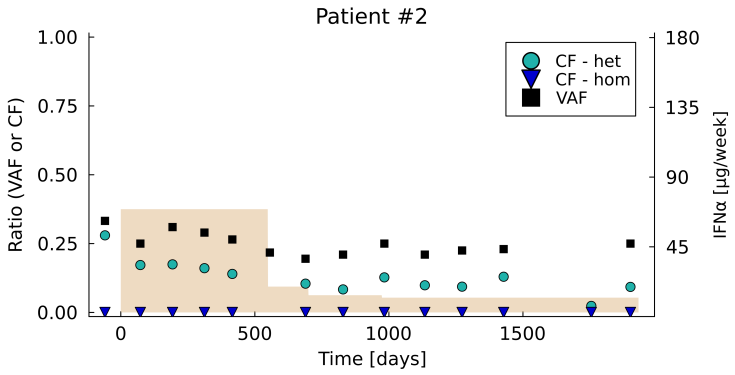

Figure A.1: Longitudinal observations of patient #2. The x-axis corresponds to the time from the start of the IFNα therapy ($t = 0$). Clinical data consist of the measurements of the VAF in mature cells (black squares), Experimental data to the heterozygous (green circles) and homozygous (blue triangles) CF in progenitor cells. The shaded beige areas correspond to the weekly dose of IFNα received over time. Some observations might have been obtained before the start of the therapy.

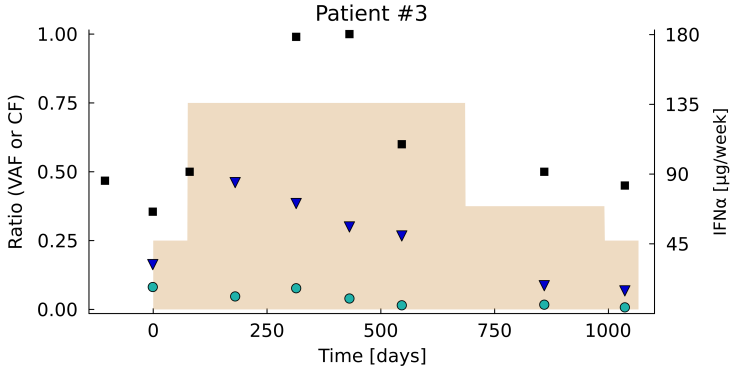

Figure A.2: Longitudinal observations of patient #3.

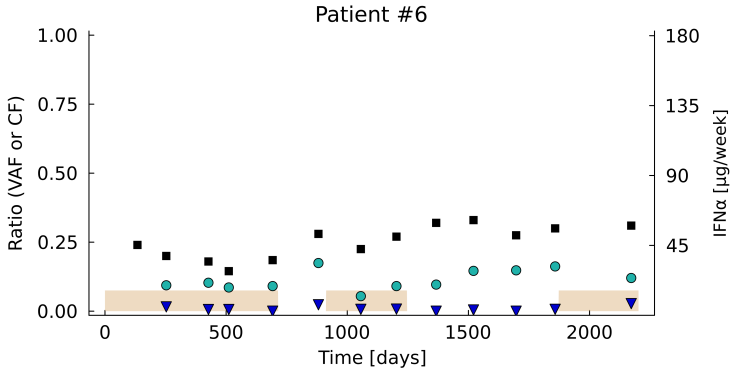

Figure A.3: Longitudinal observations of patient #6.

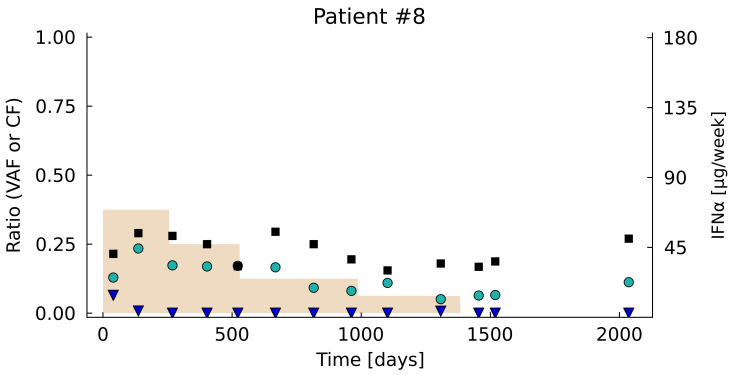

Figure A.4: Longitudinal observations of patient #8.

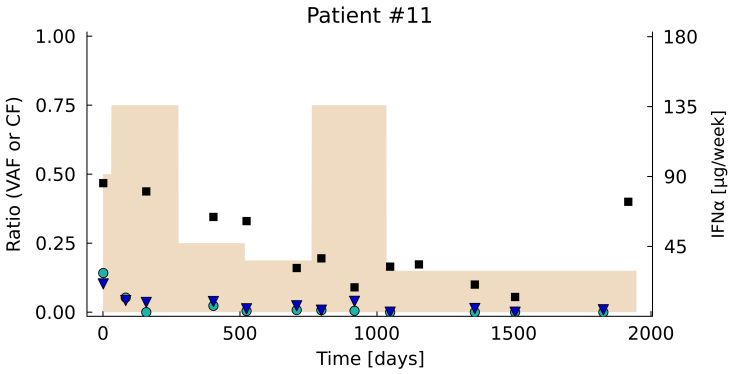

Figure A.5: Longitudinal observations of patient #11.

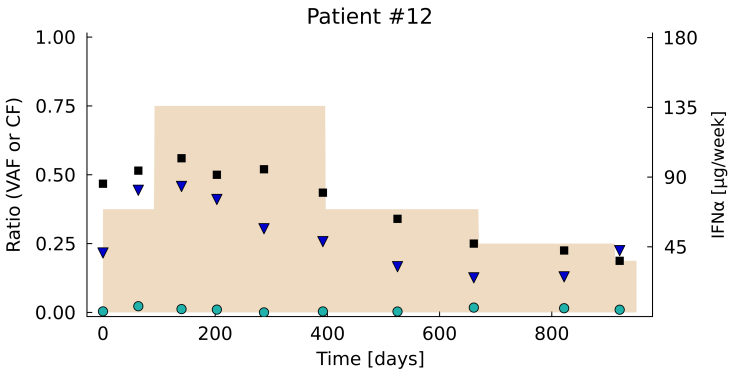

Figure A.6: Longitudinal observations of patient #12.

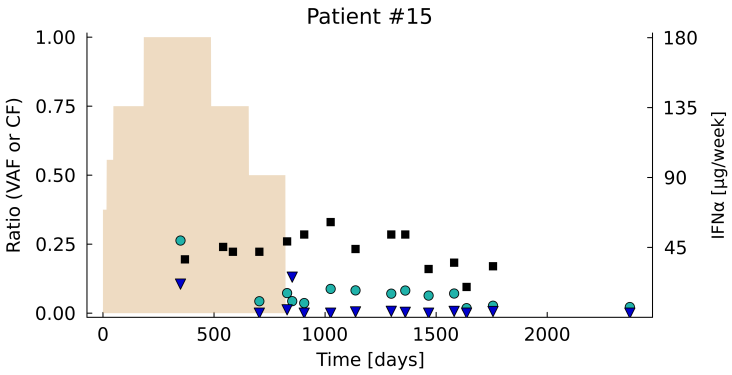

Figure A.7: Longitudinal observations of patient #15.

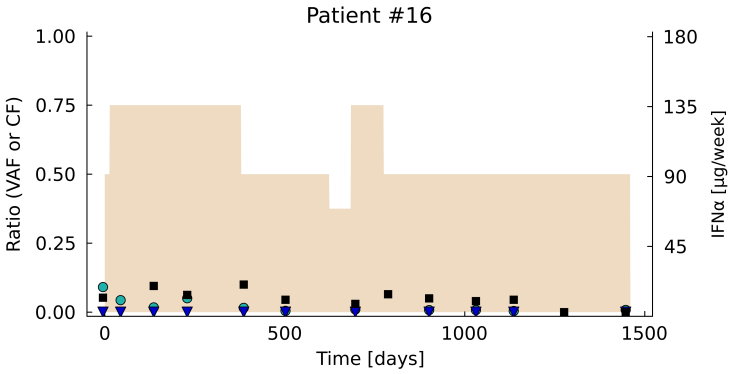

Figure A.8: Longitudinal observations of patient #16.

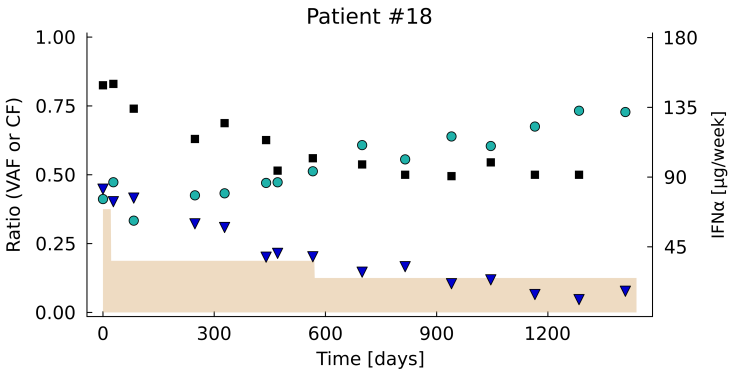

Figure A.9: Longitudinal observations of patient #18.

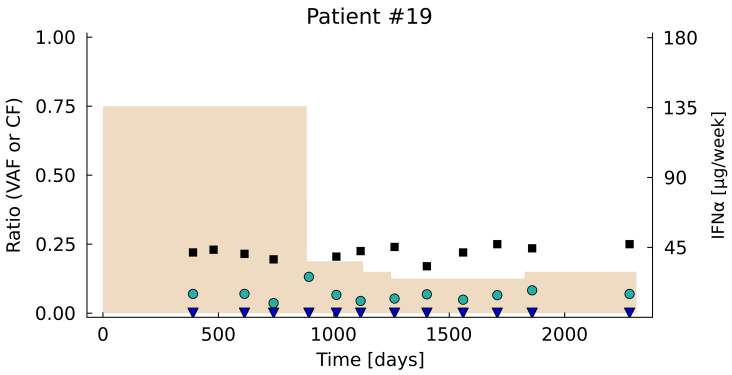

Figure A.10: Longitudinal observations of patient #19.

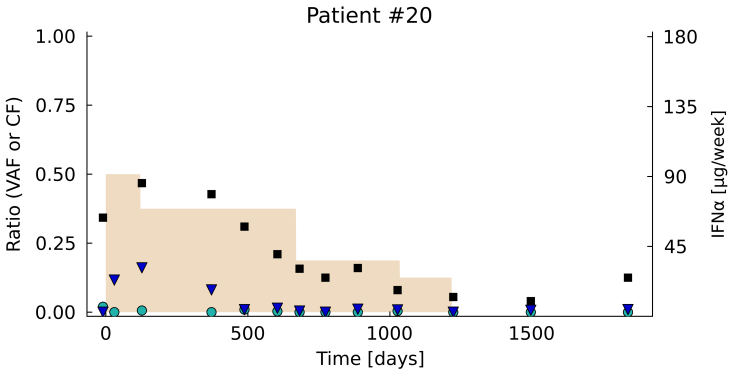

Figure A.11: Longitudinal observations of patient #20.

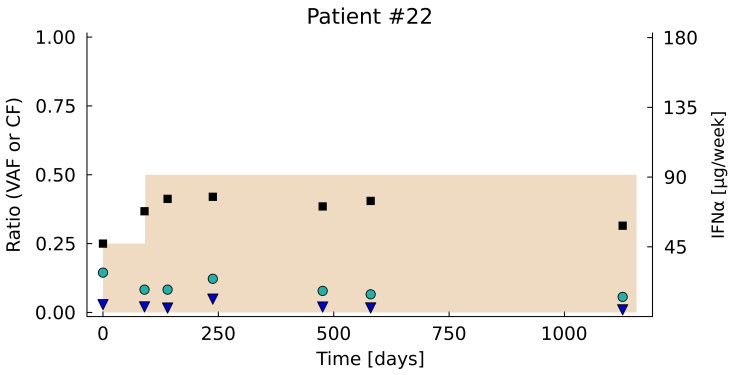

Figure A.12: Longitudinal observations of patient #22.

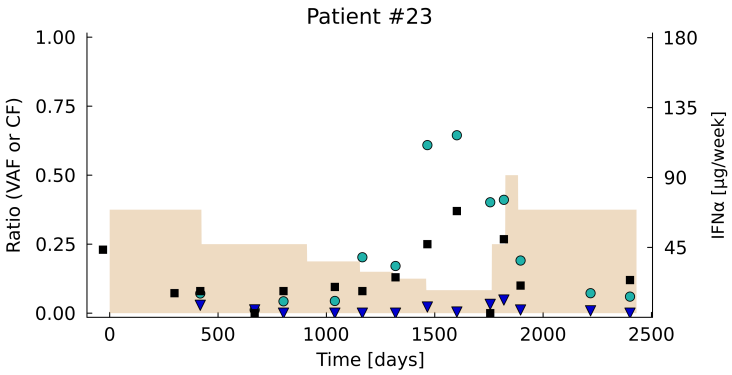

Figure A.13: Longitudinal observations of patient #23.

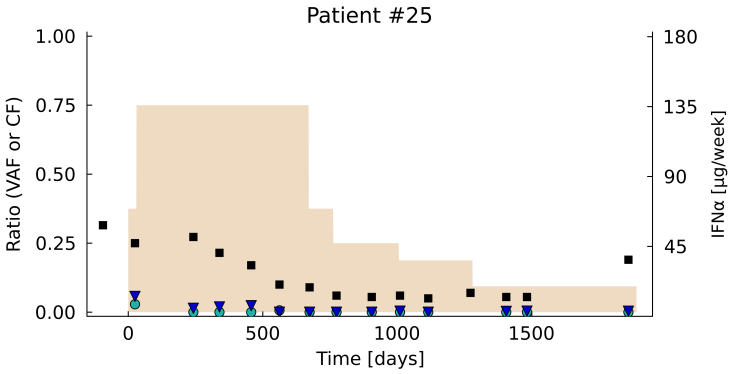

Figure A.14: Longitudinal observations of patient #25.

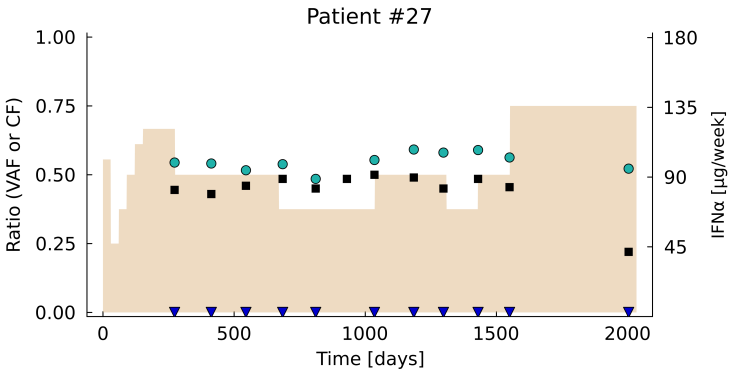

Figure A.15: Longitudinal observations of patient #27.

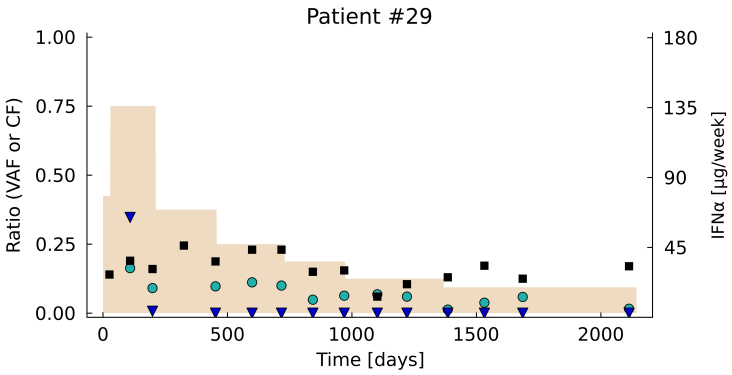

Figure A.16: Longitudinal observations of patient #29.

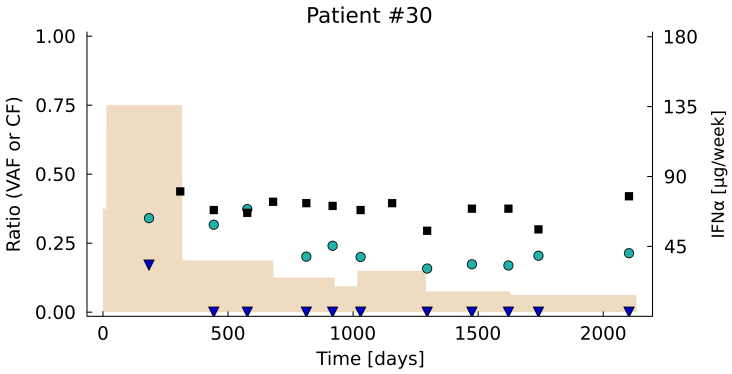

Figure A.17: Longitudinal observations of patient #30.

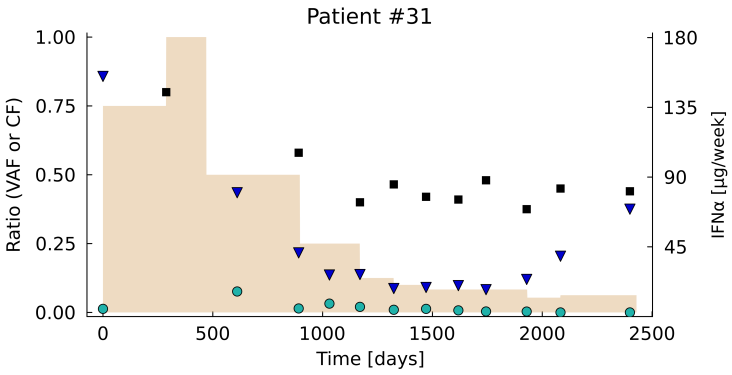

Figure A.18: Longitudinal observations of patient #31.

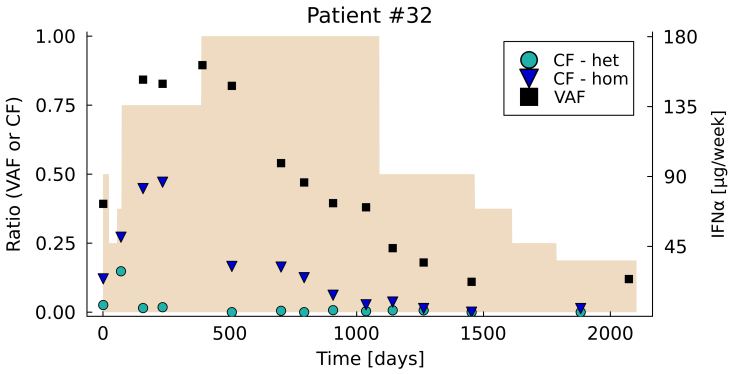

Figure A.19: Longitudinal observations of patient #32.

B Model

The model on which we base this study was first proposed by Mosca et al. [15] to describe the dynamics of mutated cells over IFNα therapy and then extended in [9] to account for dose variations during the treatment. In the original formulation from Mosca et al., three populations of cells were considered according to whether the cells are wild-type (WT) or have the $JAK2^{V617F}$ mutation in one (heterozygous, subscript het) or two (homozygous, subscript hom) alleles. These three populations were assumed to be independent. If we consider one of them (Fig. 2 - main article), their cell dynamics were described by the following system of ordinary differential equations (for clarity, we omit the subscript corresponding to the population):

$$\begin{cases} \dot{N}_q(t) &= -\gamma N_q(t) + \beta N_a(t) \\ \dot{N}_a(t) &= \gamma N_q(t) + (\alpha\Delta - \beta) N_a(t) \\ \dot{N}_i(t) &= \alpha(1-\Delta)\kappa_i N_a(t) - \delta_i N_i(t) \\ \dot{N}_m(t) &= \delta_i \kappa_m N_i(t) - \delta_m N_m(t) \end{cases} \tag{B.1}$$

where $N_q(t)$, $N_a(t)$, $N_i(t)$, and $N_m(t)$ describe respectively the numbers of quiescent HSCs, active HSCs, progenitors (that we also call immature cells) and mature cells. $\gamma N_q(t)$ and $\beta N_a(t)$ correspond to the rate at which HSCs become respectively active or quiescent, α is the division rate of active HSCs, Δ corresponds to the balance between differentiated and symmetrical division, κ_i and κ_m are the proliferative rates of immature and mature cells, respectively, δ_i is the rate constant controlling how progenitors exit their compartment to become mature cells with a death rate δ_m.
IFNα was found to act on the differentiation and quiescence exit of mutated stem cells, that is, on parameters γ and Δ [15]. In a previous study [9], after conducting a model selection procedure, we found that an affine sigmoid relation can model the impact of the variations of IFNα dose $d(t)$ on parameters Δ_{het} and Δ_{hom} through:

$$\Delta_{het} : d \longmapsto -2\left(\frac{1}{1+e^{-\rho_{het}\cdot d}} - 0.5\right)\cdot(1+\delta_{0,het}) + \delta_{0,het} \tag{B.2}$$

and equivalently for homozygous cells. The dose $d(t) \in [0,1]$ is defined as the normalized weekly averaged IFNα quantity administrated to the patient. For normalization, we divide by 180μg/week, considered the maximally tolerated dose - this maximum value seems to be a consensus but not the result of any clinical trial. $d(t)$ is a piece-wise constant input function in our model. After several biological assumptions detailed in [15, 9], the parameters to be estimated for each patient are the following:

- η_{het} and η_{hom}: the proportions of heterozygous and homozygous mutated HSCs, respectively, at the beginning of the treatment,
- γ_{het} and γ_{hom}: the rate constants of HSC quiescence exit during IFNα therapy,
- $\delta_{0,het}$, $\delta_{0,hom}$, ρ_{het} and ρ_{hom}, which describe how parameters Δ_{het} and Δ_{hom} behave depending on the IFNα dose (see eq. (B.2)). Δ_{het} and Δ_{hom} model to which extent mutated HSCs differentiate, therefore leading to an exhaustion of the mutated stem cell pool,
- $\kappa_{m,het} = \kappa_{m,hom}$, which models the proliferative advantage of mutated cells at the last stages of hematopoiesis.

C Parameter estimation

We have the data of $N = 19$ $JAK2^{V617F}$ MPN patients, as presented in section A. We denote by $\mathcal{D}$ the dataset for all 19 patients. Let us consider a patient i that we will focus on. We denote by $\mathcal{D}^{(i)}$ their dataset, and by $\mathcal{D}_{-i} = \mathcal{D} \setminus \mathcal{D}^{(i)}$ the dataset of all patients except individual i.

C.1 Hierarchical inference

The hierarchical Bayesian inference method is detailed in our previous study [9]. We provide here the information necessary for a good understanding of the methods.
$\boldsymbol{\theta^{(-i)}} = \left\{\boldsymbol{\theta^{(j)}}\right\}_{1\leq j\leq N, j\neq i}$ denotes the set of all patient parameters - except patient i - with:

$$\boldsymbol{\theta^{(j)}} = \left(\theta_1^{(j)}, \cdots, \theta_P^{(j)}\right)$$

where $P = 9$ is the number of parameters to estimate. We assume that all (except η_{het} and η_{hom}) individual parameter vectors are realizations of the same random variable of a distribution of unknown mean and variance:

$$\forall 1 \leq j \leq N, j \neq i, \forall k \in \{1, \cdots, P\}, \theta_k^{(j)} | \tau_k^{(-i)}, {\sigma_k^2}^{(-i)} \sim \mathcal{N}_{c,k}\left(\tau_k^{(-i)}, {\sigma_k^2}^{(-i)}\right) \tag{C.1}$$

where the population distribution for each component is a truncated Gaussian distribution $\mathcal{N}_{c,k}$ over a range that depends on the considered parameter k (see next paragraph), and $\boldsymbol{\tau^{(-i)}} = (\tau_1^{(-i)}, \cdots, \tau_P^{(-i)})$ and $\boldsymbol{\sigma^{2\ (-i)}} = ({\sigma_1^2}^{(-i)}, \cdots, {\sigma_P^2}^{(-i)})$ are the hyper-parameters. The prior distributions of the hyper-parameters $\tau_k^{(-i)}$ are chosen uniform, over the same ranges as for the parameters they are associated with. For each k, ${\sigma_k^2}^{(-i)}$ follows an improper prior distribution - namely, an inverse-gamma (0,0) law. Then, we can estimate the joint posterior distributions of $\boldsymbol{\theta^{(-i)}}$ and hyper-parameters $\boldsymbol{\tau^{(-i)}}$ and $\boldsymbol{\sigma^{2\ (-i)}}$, as done in [15] and detailed in [9] :

$$\begin{aligned} p\left[\boldsymbol{\theta^{(-i)}}, \boldsymbol{\tau^{(-i)}}, \boldsymbol{\sigma^{2\ (-i)}} \mid \mathcal{D}_{-i}\right] &\propto p\left[\mathcal{D}_{-i} \mid \boldsymbol{\theta}^{(1)}, \cdots, \boldsymbol{\theta}^{(i-1)}, \boldsymbol{\theta}^{(i+1)}, \cdots \boldsymbol{\theta}^{(N)}, \boldsymbol{\tau^{(-i)}}, \boldsymbol{\sigma^{2\ (-i)}}\right] \times \\ &\quad p\left[\boldsymbol{\theta}^{(1)}, \cdots, \boldsymbol{\theta}^{(i-1)}, \boldsymbol{\theta}^{(i+1)}, \cdots, \boldsymbol{\theta}^{(N)}, \boldsymbol{\tau^{(-i)}}, \boldsymbol{\sigma^{2\ (-i)}}\right] \\ &\propto \prod_{1\leq j\leq N, j\neq i} \left(p\left[\mathcal{D}^{(j)} \mid \boldsymbol{\theta}^{(j)}\right] p\left[\boldsymbol{\theta}^{(j)} \mid \boldsymbol{\tau^{(-i)}}, \boldsymbol{\sigma^{2\ (-i)}}\right]\right) p[\boldsymbol{\tau^{(-i)}}] p\left[\boldsymbol{\sigma^{2\ (-i)}}\right] \end{aligned}$$

Then, we sample from the posterior distribution using a Markov Chain Monte Carlo (MCMC) method, namely the Metropolis-Hastings within Gibbs algorithm [7, 3]. Conditionally on the hyper-parameters, patients are independent, and their parameters can be sampled using a standard Metropolis-Hasting scheme. The hyper-parameters are sampled using the Gibbs method, which consists of sampling from the marginal conditional posterior distribution of the hyper-parameters. Details of the calculations are presented in [9].
To initialize the MCMC chain, we first run an optimization algorithm - namely the CMA-ES [4, 5]. The CMA-ES is a stochastic algorithm that we use for looking at the estimator of the maximum *a posteriori*. We then use this estimator for initializing the MCMC. Furthermore, the CMA-ES algorithm also learns a covariance matrix that we choose (up to a multiplication factor) for our proposal in the Metropolis-Hasting scheme. Model calibration was achieved by implementing the previous methods in the Julia programming language. The framework used for parameter estimation is available at:

`https://gitlab-research.centralesupelec.fr/2012hermangeg/bayesian-inference`

We run our hierarchical inference method over 13 million iterations, with a burn-in length of 2 million, until achieving convergence.
After running the estimation procedure, we have for $\tau_k^{(-i)}$ and ${\sigma_k^2}^{(-i)}$ the estimate of their posterior distribution from which we estimate the posterior mean, given the observations:

$$\bar{\tau}_k^{(-i)} = \mathbb{E}[\tau_k^{(-i)} | \mathcal{D}_{-i}]$$

$$\bar{\sigma}_k^{2\ (-i)} = \mathbb{E}[\sigma^{2\ (-i)} | \mathcal{D}_{-i}]$$

These latter values will be used as prior information when considering a new patient.

C.2 Parameter estimation for a new patient

Patient i has been excluded from the cohort of patients. This patient can therefore be considered a new patient. As presented in section A, for them, we consider having only two observations of the clonal architecture, similar to what could be obtained in clinical routines.

C.2.1 Prior

$\boldsymbol{\theta^{(i)}}$ is the parameter vector of patient i:

$$\boldsymbol{\theta^{(i)}} = \left(\theta_1^{(i)}, \cdots, \theta_P^{(i)}\right)$$

For η_{het} (and η_{hom}) which correspond to the initial quantities of heterozygous (and homozygous) mutated HSCs compared to the number of wild-type HSCs, we consider a prior uniform over $[0, 3]$ (unitless parameter). For the other parameters (index k), we consider *a priori*:

$$\theta_k^{(i)} \sim \mathcal{N}_{c,k}\left(\bar{\tau}_k^{(-i)}, \bar{\sigma}_k^{2\ (-i)}\right) \tag{C.2}$$

$\mathcal{N}_{c,k}$ is a truncated Gaussian distribution over a range that depends on the considered parameter :

- For parameters $\delta_{0,het}$ and $\delta_{0,hom}$, the range is $[0.0, 0.5]$ (unitless parameters),
- For ρ_{het} and ρ_{hom}, the range is $[0, 10]$ (unitless parameters),
- For k_m, the range is $[1, 20]$ (unitless parameter),
- For $1/\gamma_{het}$ and $1/\gamma_{hom}$, the range is $[10, 300]$ (in days).

C.2.2 Bayesian Inference

We denote by $\mathcal{I}_T^{(i)}$ the set of observation times before the assimilation time T. The dataset of patient i used for estimating their parameters is:

$$\mathcal{D}_T^{(i)} = \left\{t_k^{(i)}, \hat{y}_k^{(i)}\right\}_{k \in \mathcal{I}_T^{(i)}} \bigcup \left\{\hat{n}_{k=1,wt}^{(i)}, \hat{n}_{k=1,het}^{(i)}, \hat{n}_{k=1,hom}^{(i)}\right\} \bigcup \left\{\hat{n}_{k',wt}^{(i)}, \hat{n}_{k',het}^{(i)}, \hat{n}_{k',hom}^{(i)}\right\}$$

with k' corresponding to the index of the observation made at a time close to 300 days after treatment. The posterior distribution is expressed by:

$$p[\boldsymbol{\theta_T^{(i)}}|\mathcal{D}_T^{(i)}] \propto p[\mathcal{D}_T^{(i)}|\boldsymbol{\theta_T^{(i)}}]\ p[\boldsymbol{\theta_T^{(i)}}] \tag{C.3}$$

with $p[\boldsymbol{\theta_T^{(i)}}]$ the prior expressed in the previous paragraph and $p[\mathcal{D}_T^{(i)}|\boldsymbol{\theta_T^{(i)}}]$ the likelihood.

First, we find the parameter vector $\boldsymbol{\hat{\theta}_T^{(i)}}$ which maximizes the previous posterior. $\boldsymbol{\hat{\theta}_T^{(i)}}$ is estimated using the CMA-ES algorithm [4]. Then, we run the Metropolis-Hasting algorithm, whose proposal is set to the covariance matrix learnt using the CMA-ES, and the initial state set to $\boldsymbol{\hat{\theta}_T^{(i)}}$. We run the Bayesian inference method over 1 million iterations, and verify that we achieved convergence.

In the prediction part of this study, we will study the posterior distribution of $\boldsymbol{\theta_T^{(i)}}$ according to the value of the assimilation time T.
When studying the treatment optimization or the experimental design, we consider the assimilation time $T = 600$ days, and we will set the parameter vector to the mean posterior value $\mathbb{E}[\boldsymbol{\theta_{T=600}^{(i)}}|\mathcal{D}_{T=600}^{(i)}]$.

C.2.3 Uncertainty propagation

In the prediction part of this study, we infer not only the parameter posterior distribution but also the dynamics of the mutated cells (or, more precisely, the evolution of the VAF and the CF over time). For this purpose, we sample from the posterior distribution some parameter vectors using a Monte-Carlo method and propagate the uncertainty from the input parameters to the output of the model (that is, the dynamics of the CF in each hematopoietic compartment).

C.2.4 Estimating d_{inf}

In our model, the parameter Δ_{het} depends on the dose $d \in [0,1]$ according to the equation (B.2):

$$\Delta_{het} : d \longmapsto -2\left(\frac{1}{1+e^{-\rho_{het}\cdot d}} - 0.5\right)\cdot(1+\delta_{0,het}) + \delta_{0,het}$$

The same goes for Δ_{hom}.
The parameter $\Delta_{het} \in [-1,1]$ corresponds to the balance between the differentiated and symmetrical divisions of mutated HSCs. $\Delta_{het} > 0$ means that the mutated heterozygous clone continues to expand, that is, to invade the stem cell pool. $\Delta_{het} < 0$ means that mutated HSCs encounter more differentiated divisions than symmetrical ones, so the pool of mutated HSCs will be depleted.
The necessary condition for the pool of mutated heterozygous HSCs to be potentially totally eradicated in the future is to use a dose d such that $\Delta_{het}(d) < 0$. According to our model, Δ_{het} decreases with the dose. Thus, there exists $d_{inf,het}$ such that:

$$\Delta_{het}(d_{inf,het}) = 0$$

$$\Delta_{het}(d) > 0 \text{ for } d < d_{inf,het}$$

The same goes for homozygous cells. We define $d_{inf} = \max(d_{inf,het}, d_{inf,hom})$ as the minimal dose to administer to the patient such that both the homozygous and heterozygous mutated cell could be depleted.
d_{inf} depends on parameters $\delta_{0,het}$, $\delta_{0,hom}$, ρ_{het}, and ρ_{hom}. Therefore, d_{inf} is patient-dependent.

C.2.5 Assessing the quality of the fits and predictions

For a given assimilation time T, we have estimated the model parameters (that is, their posterior distribution) based on the observations included in the dataset $\mathcal{D}_T^{(i)}$. After having propagated the uncertainties, we get the dynamics of the VAF among mature cells and the CF among progenitors. That is, for a given time, we get a distribution of the values of the VAF, and the heterozygous and homozygous CF, from which we compute (and display) the median. For each clinical and experimental data (either a CF or a VAF measurement), observed at a time t, we can then confront the experimental value to the theoretical one (i.e., the median value introduced above). For a given observation time, the distance between the experimental and the theoretical value will be the quadratic error. This error can be computed either for a VAF measurement, or an heterozygous CF, or an homozygous CF. When considering several observations, the reported error will then be the mean square error (MSE). First, the MSE could be computed based on the observations from $\mathcal{D}_T^{(i)}$. In that case, we asses how well the model fits the data (used for its calibration). The MSE can also be computed based on observations coming from the control dataset: $\mathcal{D}_c^{(i)} = \mathcal{D}^{(i)} \setminus \mathcal{D}_T^{(i)}$ (which includes all observations not used for the model calibration). In that case, we asses how well the models gives accurate predictions.

D Interrupting the therapy

This section considers the case when no IFNα is administered to the patient. It is the case when the treatment has not yet started or has been interrupted.

D.1 Criterion

We aim at optimizing the therapy from a time T to a time τ; this latter time corresponds to the end of the treatment. IFNα therapy is a long-term treatment that clinicians do not want to prolong indefinitely due to adverse effects in most cases. We aim to find a criterion for deciding when the therapy could be stopped. Such a criterion should be acceptable both for clinicians and patients.
Since MPNs are diseases that develop over a long time [17, 16], it is reasonable to choose to stop treatment even before complete eradication of the mutated HSCs, if there is a good reason to believe that the clonal development following the discontinuation of treatment is unlikely to lead to the disease recurrence (that is, the reappearance of the symptoms) during the patient's lifetime. In this work, we propose to determine, according to different criteria, when one could suggest to the clinician (and the patient) to stop the treatment.
Unless complete remission is achieved (which is difficult, if not impossible, to estimate clinically), the patient may still have several mutated stem cells prone to revert to clonal development leading to a recurrence of symptoms. Nevertheless, because of the slow clonal expansion, it can be considered that if the proportion of mutated cells remains below the threshold for symptom onset during the patient's lifetime, this will not be a problem. Of course, one cannot know how long the patient will live. One can make a conservative choice by choosing an age limit beyond 100 years, for example, which would mean wanting an almost zero risk of a possible relapse of the patient. However, such a choice might not be relevant, given the life expectancy of individuals. We thus choose to set the age limit (below which we do not want the threshold to be reached) at 90 years. This age corresponds to the life expectancy of 65-year-old individuals in 2030 in developed countries [11].
Concerning the threshold of onset of the disease, we had assumed in a previous study [8] that the disease could appear for a CF of heterozygous mutated HSCs (in patients having no homozygous clones) of 15%. That is, a VAF of 7.5% in HSCs. This latter threshold is based on the study by Dupont et al. [2].

Considering a life expectancy, at 65 years old, equal to 90 [11], we will consider interrupting the treatment of a patient at an age τ such that $\phi_\tau(t = 90 \text{ years}) = 7.5\%$ with:

$$\begin{aligned}\phi_\tau(t) &= \frac{0.5\tilde{N}_{het}(t) + \tilde{N}_{hom}(t)}{\tilde{N}_{het}(t) + \tilde{N}_{hom}(t) + N_{WT}} \\ &= \frac{0.5\tilde{N}_{het}(\tau)e^{s_{het}(t-\tau)} + \tilde{N}_{hom}(\tau)e^{s_{hom}(t-\tau)}}{\tilde{N}_{het}(\tau)e^{s_{het}(t-\tau)} + \tilde{N}_{hom}(\tau)e^{s_{hom}(t-\tau)} + N_{WT}}\end{aligned}$$

which corresponds to the VAF, among HSCs, at time t, given the quantities (or the equivalent CF) of mutated HSCs at time τ. N_{WT} is the number of wild-type HSCs, assumed to be constant and equal to 10^5 [12]. More details about the quantities involved in the expression of $\phi_\tau(t)$ are presented in the next paragraphs.

To sum up, we will choose to stop treatment at an age such that the subsequent clonal development will not lead to a VAF of 7.5% (among HSCs) before the age of 90.

D.2 Model of the clonal expansion without IFNα

First, we consider a patient having only heterozygous $JAK2^{V617F}$ clones. We assume that the clonal development after interruption of the treatment follows the same dynamics as before the treatment and that this dynamic is described by the model proposed in [8]. We assume that we remain in the case where the number of mutated cells remains sufficient for the following deterministic approximation - derived in [8] - to be valid:

$$\tilde{N}_{het}(t) = \tilde{N}_{0,het} \exp\left(s_{het}(t - t_0)\right) \tag{D.1}$$

where the fitness of the heterozygous clone was estimated to be equal to $s_{het} = 20.4\%$/year. Here, $\tilde{N}_{het}(t) = \tilde{N}_{a,het}(t) + \tilde{N}_{q,het}(t)$ corresponds to the total number of heterozygous HSCs (active and quiescent). Equation (D.1) is valid during the MPN development in the absence of IFNα therapy. We use the tilde symbol $\tilde{\circ}$ to denote a variable which dynamics is studied when the patient is not under treatment (that is, either before the start of the treatment, of after the patient has definitively interrupted the therapy).
A sufficient condition for the validity of the deterministic approximation was shown to be $\tilde{N}_{0,het} = 2,000$, but this latter choice was conservative in the sense that, even for lower values of $\tilde{N}_{0,het}$, the approximation error was low [8].

Now, we consider the more general case of a patient having both heterozygous and homozygous clones that can develop in parallel. In that case, the heterozygous CF among HSCs is defined by:

$$\begin{aligned} CF_{het}(t) &= \frac{\tilde{N}_{het}(t)}{\tilde{N}_{het}(t) + \tilde{N}_{hom}(t) + N_{WT}} \\ &= \frac{\tilde{N}_{q,het}(t) + \tilde{N}_{a,het}(t)}{\tilde{N}_{q,het}(t) + \tilde{N}_{a,het}(t) + \tilde{N}_{q,hom}(t) + \tilde{N}_{a,hom}(t) + N_{WT}} \end{aligned} \tag{D.2}$$

And the VAF among HSCs:

$$VAF(t) = \frac{0.5\ \tilde{N}_{het}(t) + \tilde{N}_{hom}(t)}{\tilde{N}_{het}(t) + \tilde{N}_{hom}(t) + N_{WT}} \tag{D.3}$$

In all this study, we consider that the number of the WT HSCs is constant and equal to $N_{WT} = 10^5$ [12]. In particular, we do not assume that, during the clonal expansion, mutated cells might replace WT cells. On the contrary, we consider that mutated HSCs expand in parallel to the WT, potentially conquering other hematopoietic niches [6], such that the number of WT (normal) HSCs remains constant. To note that the hypothesis of a constant number of WT HSCs during a clonal expansion of mutated HSCs was also done by Michor et al. [14] when studying the dynamics of chronic myeloid leukemia. We assume that the expansion of the malignant homozygous mutated cells will follow the same dynamics as the heterozygous one:

$$\tilde{N}_{hom}(t) = \tilde{N}_{0,hom} \exp\left(s_{hom}(t - t_0)\right) \tag{D.4}$$

with a fitness s_{hom} higher than for the heterozygous case [17]. We estimate the value of the homozygous fitness in the next section.
Then, we get the expression of the VAF among HSC over time $t \geq t_0$, given the values at time t_0:

$$VAF(t) = \frac{0.5\ \tilde{N}_{het}(t_0)e^{s_{het}(t-t_0)} + \tilde{N}_{hom}(t_0)e^{s_{hom}(t-t_0)}}{\tilde{N}_{het}(t_0)e^{s_{het}(t-t_0)} + \tilde{N}_{hom}(t_0)e^{s_{hom}(t-t_0)} + N_{WT}} \tag{D.5}$$

D.3 Estimating the fitness of the $JAK2^{V617F}$ homozygous clone

D.3.1 Approach

To describe the clonal expansion without IFNα, we use the model we previously studied in [8]. From our previous work, we also estimated the fitness of the heterozygous clone to be equal to $s_{het} = 20.4\%$/year. However, the study was not conducted for patients with homozygous clones, so we do not have an estimation of s_{hom}. We expect to have $s_{hom} > s_{het}$ [17]. We consider that:

$$s_{hom} = \beta\ s_{het}$$

with $\beta > 1$. To estimate s_{hom} (or, equivalently, β), we will use the data from Williams et al. [17] (Fig. D.1). In their study, they had some patients with heterozygous mutated clones and some others with homozygous mutated clones. Using a model they calibrated based on the whole genome sequencing of progenitor cells and the subsequent construction of phylogenetic trees, they inferred the fitness S_i of mutated $JAK2^{V617F}$ clones for different patients (index i). From their study, we can get their estimated $S_{i,het}$ for $1 \leq i \leq n_{het}$ and $S_{i,hom}$ for $1 \leq i \leq n_{hom}$, with n_{het} and n_{hom} the number of heterozygous and homozygous patients they studied, respectively. If we note $\tilde{S}_{het}$ the median

Figure D.1: Data from Williams et al. [17]. From their article, we extracted the mean value of their so-called S parameter, which corresponds to the fitness of a mutated clone. We display the value of S according to whether it refers to a $JAK2^{V617F}$ heterozygous clone or a homozygous one. There is a trend to have higher fitness in the homozygous condition ($p = 0.1535$ with a Mann-Whitney test [13]).

heterozygous fitness and $\tilde{S}_{hom}$ the median homozygous fitness, we could compute $\beta' = \tilde{S}_{hom}/\tilde{S}_{het}$, and, in a naive approach, set $\beta = \beta'$. Yet, this first estimation of β would be too approximate since their model differs significantly from ours. Indeed, Williams et al. assume the HSC pool to be of constant size, and, therefore, that mutated cells take the place of WT cells during their expansion. On the contrary, we assume in our model that we have a constant number of WT cells and that the mutated cells expand without replacing the former. To circumvent the difficulty related to the fact that our models are different, we will try to find a relation $f : S_{het,i} \longmapsto s_{het,i}$ such that $s_{het,i}$ is consistent with the fitness used in our model. Then, we could find a better estimation for β using:

$$\beta \approx \frac{f(\tilde{S}_{het})}{f(\tilde{S}_{hom})} \tag{D.6}$$

D.3.2 Finding the relation $f : S_{het} \longmapsto s_{het}$

Here, we will approximate a relation that links the so-called "fitness of clone" S of Williams et al. [17] to our fitness s. In this paragraph, we consider the case of heterozygous mutated cells and omit the subscript het for clarity. In Williams et al.'s model, the number of mutated cells $N(t)$ follows the differential equation:

$$\frac{dN}{dt} = N(t)\alpha\varsigma\left(1 - \frac{N(t)}{N_{tot}}\right) \tag{D.7}$$

and they define:

$$S = \exp(\alpha\varsigma) - 1$$

where ς is the selective advantage (in their paper, they note it actually s but, to avoid the confusion with our fitness parameter, we note it ς), α corresponds to a division rate as in [8], and N_{tot} is the total size of the HSC pool (WT and mutated) assumed to be constant. In our case, on the contrary, we have $N_{tot} = N_{WT} + N(t)$ with $N(t)$ the number of mutated cells. In our model, if we differentiate equation (D.1), we get:

$$\frac{dN}{dt} = s\ N(t) \tag{D.8}$$

By equalizing equations (D.7) and (D.8), we get:

$$s = \log(1 + S)\left(1 - \frac{N(t)}{N_{tot}}\right)$$

If we assume that the CF among HSCs $N(t)/N_{tot}$ is approximately equal to the one among progenitors η (that is, the CF that can be measured by Williams et al.), we get:

$$s \approx \log(1+S)(1-\eta(t)) \tag{D.9}$$

If we integrate the previous equation from the acquisition time to the sampling time, and assume a linear clonal expansion (which we acknowledge is a rough approximation), we get:

$$s \approx \log(1+S)\left(1-\frac{\hat{\eta}}{2}\right) = f(S) \tag{D.10}$$

with $\hat{\eta}$ the CF among progenitor cells measured at the observation time.

D.3.3 Results

For each individual i from the cohort of Williams et al. [17], we have their estimate S_i and we can estimate the progenitor CF $\hat{\eta}_i$ at sampling time by counting the numbers of mutated and WT individual colonies at the tips of the phylogenetic tree branches. Below, we report the values from Williams et al. that we use for this analysis. The data for the patients having heterozygous but no (or negligible) homozygous clones are the following:

- PD6646: S = 119 %/year (clade JAK2, DNMT3A) - $\hat{\eta}$ = 56.7%
- PD5179: S = 116 %/year (clade JAK2, 1q+, 9q-, 9+) - $\hat{\eta}$ = 96.7%
- PD6629: S $\approx$ 66 %/year (clade DNMT3A, JAK2, TET2, and clade DNMT3A, JAK2) - $\hat{\eta}$ = 43.8%
- PD7271: S = 73 %/year (clade JAK2) - $\hat{\eta}$ = 21.6%
- PD9478: S = 71 %/year (clade JAK2, DNMT3A) - $\hat{\eta}$ = 89.5%
- PD5163: S = 45 %/year (clade JAK2) - $\hat{\eta}$ = 8.6%
- PD5117: S = 18 %/year (clade JAK2) - $\hat{\eta}$ = 55.7%

For patient PD6629, Williams et al. have two estimations of S according to the considered clade (S = 90 %/year for the clade DNMT3A, JAK2, TET2, and S = 41 for the clade DNMT3A, JAK2), we consider the mean value.

For patients having homozygous clones but no (or negligible) heterozygous ones, the data are the following:

- PD4781: S=114%/year (clade TET2, JAK2, 9pUPD, 7p-, 7p+) - $\hat{\eta}$ = 97.44%
- PD5847: S $\approx$ 122.5 %/year (clade TET2, JAK2, 9pUPD and clade JAK2, 9pUPD) - $\hat{\eta}$ = 80.2%
- PD5182: S = 132 %/year (clade 9pUPD, JAK2) - $\hat{\eta}$ = 34.38%

For patient PD5847, Williams et al. have two estimations of S according to the considered clade (S = 187 %/year for the clade TET2, JAK2, 9pUPD, and S = 58 for the clade JAK2, 9pUPD), we consider the mean value.

From the previous values and using eq. (D.10), we can compute a fitness $s_i = f(S_i)$ for each patient i from Williams et al. [17]. Results are displayed in figure D.2.
Then, we estimate our parameter β by computing the ratio between the median of the s values for homozygous patients ($\tilde{s}_{hom}$ = 47.9 %/year), and the median of the s values for the heterozygous patients ($\tilde{s}_{het}$ = 39.6 %/year). We find β = 1.21.

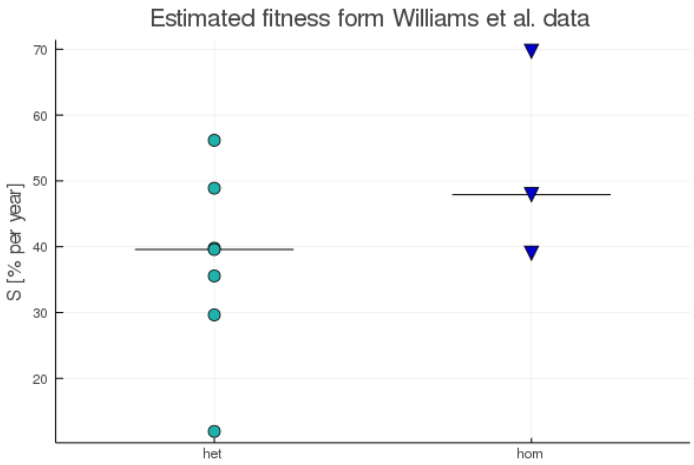

Figure D.2: Estimation of a fitness value s for each patient from Williams et al. [17] using eq. (D.10).

E Optimizing the therapy

E.1 Grid search of the optimal parameters

For a given patient, we estimated their parameter vector $\boldsymbol{\theta}$ as presented in § C.2.2, here with the assimilation time $T = 600$ days. The parameter vector entirely describes the patient's response to the treatment, for any potential dose $d(t) \in [0, 1]$ over time t. We consider three therapeutic strategies (index s), as presented in §2.3.2 in the main text:

- $s = 1$ corresponding to the constant strategy,
- $s = 2$ corresponding to the periodic strategy,
- $s = 3$ corresponding to the decreasing strategy (see also § E.3).

We note $\boldsymbol{X} \in \mathbb{R}^3$ the parameter vector of dimension 3 associated with the strategy:

$$\boldsymbol{X} = \left(\bar{d}, L, \lambda\right)$$

As we have defined it - and without any constraints on parameters L and λ - the constant strategy would be a special case of both the decreasing and periodic strategies. The constant strategy is the limiting case of the decreasing strategy when $\lambda = 1$, and the limiting case of the periodic strategy for $L \longrightarrow +\infty$. In practice, given that we study times on the scale of human life, $+\infty$ could be replaced by any high enough time value so that we would still have $\boldsymbol{X} \in \mathbb{R}^3$.
The choice of $\boldsymbol{X}$ entirely characterizes which dose would be administered to the patient for $t \geq T$, if the treatment were not interrupted. That is:

$$d_s : \left| \begin{array}{ccc} \mathbb{R}^3 \times [T, +\infty[& \longrightarrow & [0, 1] \\ (\boldsymbol{X}, t) & \longmapsto & d_s(t) \end{array} \right.$$

Then, the values of $\boldsymbol{\theta}$ and $\boldsymbol{X}$ entirely characterize the response to the treatment for any time $t \geq T$. In particular, we infer the dynamics of the VAF among HSCs. By applying the criterion presented in § D, we can estimate the time τ when the treatment could be interrupted. To note that, to apply this criterion, we also need to know the age of the patient at the beginning of their therapy (see Tab. A.1). The interruption time is thus a function:

$$\tau_s : \left| \begin{array}{ccc} \mathbb{R}^3 & \longrightarrow & [T, +\infty[\\ \boldsymbol{X} & \longmapsto & \tau \end{array} \right.$$

We omit to precise that τ also depends on the patient's parameter vector (and their age) since these latter values are supposed to be known, and because they do not come into play in the optimization problem we study here.

We consider four scenarios of dose-toxicity (index x) as presented in §2.3.3 in the main text:

- $x = 1$ corresponding to the linear relation,
- $x = 2$ corresponding to the convex relation,
- $x = 3$ corresponding to the concave relation,
- $x = 4$ corresponding top the composite relation (see also § E.4).

We define the toxicity as a function of the dose:

$$z_x : \left| \begin{array}{ccc} [0,1] & \longrightarrow & \mathbb{R}^+ \\ d & \longmapsto & z_x(d) \end{array} \right.$$

Finally, we define the toxicity-related amount of IFNα administered from T to the end of the therapy:

$$M_x : \left| \begin{array}{ccc} \mathbb{R}^3 & \longrightarrow & \mathbb{R}^+ \\ \boldsymbol{X} & \longmapsto & \int_T^{\tau_s(\boldsymbol{X})} z_x\left(d_s(\boldsymbol{X}, t)\right)\ dt \end{array} \right. \tag{E.1}$$

Our optimization problem to solve is to find the parameter vector $\boldsymbol{X}_x^*$ which minimizes the function M_x for a given dose-toxicity scenario x.
First, we can split the problem according to the therapeutic strategy s. For a given therapeutic strategy s, we denote by $S_s \subset \mathbb{R}^3$ the set of the authorized values, and we will look for:

$$\boldsymbol{X}_{s,x}^* = \underset{\boldsymbol{X} \in S_s}{\operatorname{argmin}}\ M_x(\boldsymbol{X}) \tag{E.2}$$

$\boldsymbol{X}_{s,x}^*$ corresponds to the optimal parameter vector of strategy s, for the dose-toxicity scenario x. Previously, we stated that the constant strategy would be a special case of the decreasing or periodic ones if there were no constraints on the parameters. Thus, we impose to have $S_i \bigcap S_j = \emptyset$ for $1 \leq i < j \leq 3$. We consider S_s as a discrete set of values rather than a continuous subspace of $\mathbb{R}^3$, so the optimization problem to solve will consist of looking at all potential values $\boldsymbol{X} \in S_s$ to find the one which minimizes $M_x(\boldsymbol{X})$. We refer to this procedure as "grid search". It would have been feasible to solve the optimization problem numerically even if S_s were continuous. Considering S_s as a discrete set of values will be convenient for looking for a trade-off strategy, as explained in the next section. Moreover, the parameter vector $\boldsymbol{X}$ characterizes a therapeutic strategy; it would not be relevant to explore all potential values since the clinician could not apply exactly the dose strategy as we would recommend it. For example, it would not make sense for the clinician to have a precision of the day for the period L, or a precision of 1μg/week (i.e., 1/180 for the normalized dose) for the choice of the dose $\bar{d}$. We consider the following potential values:

$$\bar{\boldsymbol{d}} = (d_{inf}, d_{inf} + 0.02, d_{inf} + 0.04, \cdots, 0.98, 1.0)$$

$$\boldsymbol{L} = (30, 60, \cdots, 24 \times 30)$$

$$\boldsymbol{\lambda} = (0.05, 0.1, \cdots, 0.90, 0.95)$$

To note that, already with the choice of $\bar{\boldsymbol{d}}$, we consider more values than can be used in clinical routine. d_{inf} is specific to the patient, that is, a function of $\boldsymbol{\theta}$, as presented in § C.2.4. The period L is in days. We have $S_3 = \bar{\boldsymbol{d}} \times \boldsymbol{L} \times \boldsymbol{\lambda}$, $S_2 = \bar{\boldsymbol{d}} \times \boldsymbol{L} \times \{1.0\}$, and $S_1 = \bar{\boldsymbol{d}} \times \{+\infty\} \times \{1.0\}$. For this latter, the singlet $\{+\infty\}$ could be replaced by any high enough value, for example, a time length that exceeds the maximal possible lifetime.

Once we have found the parameter vector which minimizes M_x for a given dose-toxicity scenario x and a given therapeutics strategy s, we can also look for the best strategy over the three considered. That is, we look for the following:

$$\boldsymbol{X}_x^* = \underset{\boldsymbol{X} \in S}{\operatorname{argmin}}\ M_x(\boldsymbol{X}) \tag{E.3}$$

where $S = S_1 \bigcup S_2 \bigcup S_3$. The corresponding optimal strategy index s is such that $\boldsymbol{X}_x^* \in S_s$.
In this section, we only wanted to minimize the toxicity-related amount of IFNα given the dose-toxicity scenario x. When this latter is not known in advance, we have to search for a trade-off strategy.

E.2 Trade-off strategy

The best strategy for one dose-toxicity scenario is unlikely to be the best one for another scenario. Without prior knowledge of how IFNα toxicity increases with the dose, we must look for a compromise. Values of the toxicity-related amount of IFNα, as given by (E.1), are not comparable for two different toxicity relations. We consider S the set of all possible values for $\boldsymbol{X}$, over the three therapeutic strategies we consider. We denote by $|S| \in \mathbb{N}$ its cardinal, that is, the number of all potential values. Each value $\boldsymbol{X}_i \in S$, for $1 \leq i \leq |S|$, can be sorted according to the value $M_x(\boldsymbol{X}_i)$, for a given $1 \leq x \leq 4$. We note $n_x(\boldsymbol{X})$ the rank, with $n_x = 1$ being the best rank, and $q_x(\boldsymbol{X}) = n_x(\boldsymbol{X})/|S| \in [0,1]$ (also expressed in % when presenting the results). We note $q(\boldsymbol{X}) = \max_{1 \leq x \leq 4} (q_x(\boldsymbol{X}))$. Then, finding the trade-off strategy is equivalent to finding:

$$\boldsymbol{X}^* = \underset{\boldsymbol{X} \in S}{\operatorname{argmin}}\ q(\boldsymbol{X}) \tag{E.4}$$

E.3 Note about the decreasing strategy

The decreasing strategy is formulated in the article by:

$$d(t) = \begin{cases} \bar{d} & \text{for } t \in [T, T+L], \\ \lambda d(t-L) & \text{for } t \in [T+L, \tau] \end{cases} \tag{E.5}$$

This is a recursive formulation. An other way to express it without self-referring is as follows:

$$d(t) = \bar{d} \cdot \lambda^{n(t)} \text{ for } t \in [T, \tau]$$

with $n(t) = \lfloor \frac{t-T}{L} \rfloor$ (where $\lfloor x \rfloor$ gives the integer part of x).

E.4 Note about the composite dose-toxicity relation

The composite dose-toxicity is defined in the article as followed:

$$z(d) = \frac{5\sqrt{5}}{9}\sqrt{d-0.1}\ \mathbb{1}_{d \in [0.1, 0.55]} + \frac{5}{4\sqrt{5}}\frac{1}{\sqrt{1-d}}\ \mathbb{1}_{d \in [0.55, 1]} \tag{E.6}$$

Here, we will detail the construction of this relation, and particularly the choice of the numerical values involved in that relation.
The composite relation is a more complex relation than the linear, convex, or concave ones, with:

- first, a low threshold d_{low} under which there is no toxicity: $z(d) = 0$ for $d < d_{low}$,
- second, a steep increase leading to a plateau like level, when a second threshold d_{up} is reached. We choose to model this increase by a relation close to our concave relation, that is, $z(d) \propto \sqrt{d - d_{low}}$ for $d \in [d_{low}, d_{up}[$ (ensuring the continuity of the function for $d = d_{low}$ with $z(d_{low}) = 0$),
- and finally, an increase of the toxicity towards an infinite value at the maximal considered dose $d_{max} = 1$. Several functions could have been chosen to model this behavior. In addition to reaching an infinite value for $d = d_{max}$, we also want the normalization $\int_0^1 z(d)\ \mathrm{d}d = 1$. Such normalization requires to be able to integrate a function which diverges at a finite value. For that reason, a usual choice of function would be to consider that $z(d) \propto \frac{1}{\sqrt{d_{max} - d}}$ for $d \in [d_{up}, d_{max}]$.

Then, the choice for the composite relation would be:

$$z(d) = \begin{cases} 0 & \text{if } d \in [0, d_{low}[\\ \zeta_1 \sqrt{\frac{d - d_{low}}{d_{up} - d_{low}}} & \text{if } d \in [d_{low}, d_{up}[\\ \zeta_2 \sqrt{\frac{d_{max} - d_{up}}{d_{max} - d}} & \text{if } d \in [d_{up}, d_{max}] \end{cases}$$

with ζ_1, ζ_2, d_{low} and d_{up} to be determined ($d_{max} = 1$). Previous equation already accounts for two conditions : 1) continuity at $d = d_{low}$, and 2) divergence at $d = d_{max}$.
In addition to both conditions, we want: 3) continuity at $d = d_{up}$, that is:

$$\zeta_1 = \zeta_2 := \zeta \tag{E.7}$$

4) continuity of the derivative at $d = d_{up}$, which leads to:

$$\frac{1}{2(d_{up} - d_{low})} = \frac{1}{2(1 - d_{up})}$$

that is:

$$d_{up} = 0.5(1 + d_{low}) \tag{E.8}$$

and finally, 5) normalization:

$$\int_0^1 z(d)\ \mathrm{d}d = 1 \tag{E.9}$$

We have:

$$\begin{aligned}
\int_0^1 z(d)\ \mathrm{d}d &= \int_0^{d_{low}} z(d)\ \mathrm{d}d + \int_{d_{low}}^{d_{up}} z(d)\ \mathrm{d}d + \int_{d_{up}}^1 z(d)\ \mathrm{d}d \\
&= 0 + \frac{\zeta}{\sqrt{d_{up} - d_{low}}} \int_0^{d_{up} - d_{low}} \sqrt{d}\ \mathrm{d}d + \zeta\sqrt{1 - d_{up}} \int_0^{1 - d_{up}} \frac{1}{\sqrt{d}}\ \mathrm{d}d \\
&= \frac{\zeta}{\sqrt{d_{up} - d_{low}}} \frac{2}{3}(d_{up} - d_{low})^{3/2} + 2\zeta(1 - d_{up}) \\
&= \zeta\left(\frac{2}{3}(d_{up} - d_{low}) + 2(1 - d_{up})\right)
\end{aligned}$$

The previous conditions are not sufficient to allow determining a value of each our parameters; there is still one degree of liberty left. We choose to set $d_{low} = 0.1$ (corresponding to 18 μg/week).
Then, from eq. (E.8) , we get $d_{up} = 0.55$ (that is, $d_{up} - d_{low} = 0.45 = 1 - d_{up}$).
Finally, $\int_0^1 z(d)\ \mathrm{d}d = 0.45\zeta\left(\frac{2}{3} + 2\right) = \frac{6}{5}\zeta$ so that $\zeta = \frac{5}{6}$ according to condition (E.9).
Using these numerical values, the composite dose-toxicity can be written as:

$$z(d) = \begin{cases} 0 & \text{if } d \in [0, 0.1[\\ \frac{5}{6}\sqrt{\frac{d - 0.1}{9/20}} & \text{if } d \in [0.1, 0.55[\\ \frac{5}{6}\sqrt{\frac{9/20}{1 - d}} & \text{if } d \in [0.55, 1] \end{cases}$$

or equivalently, $z(d)$ can be given by eq. (E.6).

F Estimating the best timing for measuring the clonal architecture

Our recommendations must be based on accurate estimations of the individual model parameters for validity. The clinician might play an active role not only in the prescription of the IFNα dose and the monitoring of the hematological response but also in the choice of the dates at which the clonal architecture of progenitor cells is measured. Indeed, by default, we chose to consider that the second measurement (the first one being at the start of the therapy) of the CF among immature cells is obtained about 300 days after the start of the therapy. This choice is consistent with another study exploring the effect of combining IFNα with ruxolitinib on MPN patients, where the clonal architecture could only be measured twice, and the second time-point was chosen about 300 days after the start of the therapy [10]. In this part, we want to explore the relevance of this choice.
To this end, we will conduct a study based on a synthetic dataset derived from the three patients #18, 12, and 32, for whom we estimated the model parameters.

For a given patient i, we estimated their parameter vector $\boldsymbol{\theta^{(i)}}$ as presented in § C.2.2, here with the assimilation time $T = 600$ days. We assume these values to be the true ones. The parameter vector entirely describes the patient's response to the treatment for any potential dose $d(t) \in [0, 1]$ over time t. We simulate, from the model and the value for $\boldsymbol{\theta^{(i)}}$, the response to the treatment for $t \in [0, 600]$ and the dose $d(t)$ received by the considered patient. We get the simulated dynamics of the VAF $y_{\boldsymbol{\theta^{(i)}}}(t)$ and the heterozygous $z_{\boldsymbol{\theta^{(i)}},het}(t)$ and homozygous $z_{\boldsymbol{\theta^{(i)}},hom}(t)$ CF over time t. We call the latter values the true ones (or the theoretical ones). We will try to retrieve these values using our inference method. In particular, we will explore the influence of the choice of the time point T_{obs} of the second observed CF. For that purpose, we simulate synthetic datasets (Fig. F.1-i).
For the considered patient i, the (clinical) VAF was measured at different time points: $\left\{t_k^{(i)}\right\}_{k\in\mathcal{I}^{(i)}_{T=600}}$.
We consider then the simulated values of the VAF $y_{\boldsymbol{\theta^{(i)}}}(t_k^{(i)})$ for $k \in \mathcal{I}^{(i)}_{T=600}$. From these latter, we generate noisy VAF measurements $\hat{y}_k^{(i)}$ using eq. (A.1) (pseudo-observations). Then, we build the following synthetic datasets, according to the choice of the time $T_{obs} \in \{1, \dots, 600\}$, which corresponds to the time when the second (pseudo-)observation of the clonal architecture would be made (Fig. F.1-ii):

$$\mathcal{D}^{(i)}_{T_{obs}} = \left\{t_k^{(i)}, \hat{y}_k^{(i)}\right\}_{k\in\mathcal{I}^{(i)}_{T=600}} \bigcup \left\{z_{\boldsymbol{\theta^{(i)}},het}(0), z_{\boldsymbol{\theta^{(i)}},hom}(0)\right\} \bigcup \left\{z_{\boldsymbol{\theta^{(i)}},het}(T_{obs}), z_{\boldsymbol{\theta^{(i)}},hom}(T_{obs})\right\}$$

We conduct 600 parameter estimation procedures (Fig. F.1-iii), one for each $\mathcal{D}^{(i)}_{T_{obs}}$, $1 \leq T_{obs} \leq 600$, to estimate the parameter vector $\boldsymbol{\theta}^{(i)}_{T_{obs}}$ for which the posterior density function is maximal. For each $T_{obs} \in \{1, \dots, 600\}$, we estimate the parameter $\boldsymbol{\hat{\theta}^{(i)}_{T_{obs}}}$ which maximizes the posterior:

$$p[\boldsymbol{\theta^{(i)}_{T_{obs}}}|\mathcal{D}^{(i)}_{T_{obs}}] \propto p[\mathcal{D}^{(i)}_{T_{obs}}|\boldsymbol{\theta^{(i)}_{T_{obs}}}]\ p[\boldsymbol{\theta^{(i)}_{T_{obs}}}] \tag{F.1}$$

with $p[\boldsymbol{\theta^{(i)}_{T_{obs}}}]$ the prior expressed in § C.2.1.
Since the optimization problem has to be repeated 600 times for each patient, we solve numerically with an efficient algorithm, namely the CMA-ES (Covariance Matrix Adaptation - Evolution Strategy) algorithm [4, 5]. $\boldsymbol{\hat{\theta}^{(i)}_{T_{obs}}}$ is estimated numerically using the CMA-ES algorithm. From our model and the value of $\boldsymbol{\hat{\theta}^{(i)}_{T_{obs}}}$, we get the inferred dynamics of the heterozygous $z_{\boldsymbol{\hat{\theta}^{(i)}_{T_{obs}}},het}(t)$ and homozygous $z_{\boldsymbol{\hat{\theta}^{(i)}_{T_{obs}}},hom}(t)$ CF, that we can confront to the theoretical ones, that is, to the target ones obtained by simulation (Fig. F.1-iv). For that purpose, we define the following prediction error:

$$\begin{aligned}\varepsilon(T_{obs}) &= \int_0^{T=600} |z_{\boldsymbol{\hat{\theta}^{(i)}_{T_{obs}}},het}(t) - z_{\boldsymbol{\theta^{(i)}},het}(t)| + |z_{\boldsymbol{\hat{\theta}^{(i)}_{T_{obs}}},hom}(t) - z_{\boldsymbol{\theta^{(i)}},hom}(t)|\ dt \\ &\approx \sum_{k=1}^{600} |z_{\boldsymbol{\hat{\theta}^{(i)}_{T_{obs}}},het}(k) - z_{\boldsymbol{\theta^{(i)}},het}(k)| + |z_{\boldsymbol{\hat{\theta}^{(i)}_{T_{obs}}},hom}(k) - z_{\boldsymbol{\theta^{(i)}},hom}(k)|\end{aligned} \tag{F.2}$$

Then, we search for the (pseudo-)observation time T^*_{obs} which minimizes the previous error:

$$T^*_{obs} = \underset{1 \leq T_{obs} \leq 600}{\operatorname{argmin}} \ \varepsilon(T_{obs}) \tag{F.3}$$

From this study, we could then discuss whether there would be some choices that are better than others (and consistent among the three patients we consider), to deduce the best timing for the second measurement of clonal architecture.

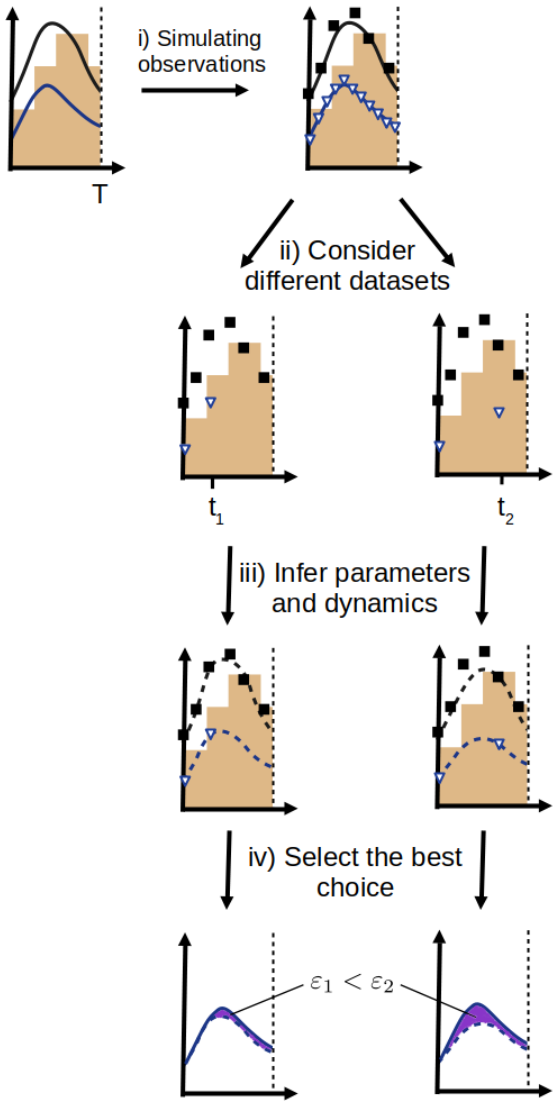

Figure F.1: Illustration of the experimental design method. We consider that we know the true parameter vector for a given patient, that is, the parameter vector $\boldsymbol{\theta}$. First, we simulate data (i), consisting of VAF measurements, as well as daily observations of the clonal architecture (pseudo-observations). Note that we simulate as many VAF pseudo-observations as we actually have for the patient and at the same observation times. For clarity, we do not represent all the data points for the CF. We consider different potential pseudo datasets for the parameter estimation procedure; these peudo-datasets are built with all VAF pseudo-observations and only two pseudo-observations of the CF (ii). The pseudo-datasets differ according to the choice of the second pseudo-observation time T_{obs} of the CF, here t_1 *vs* t_2. For each pseudo-dataset, we infer the model parameters, and, thus, the cell dynamics over IFNα (iii). Then, we compare the error between the inferred CF dynamics and the true one (iv).

G Detailed results

Our study is organized into three parts, and so are our results. In § G.1, we present the results of the prediction, in § G.2 how the therapy could be optimized, and in § G.3 how to choose the best timing for measuring the clonal architecture. We present the results separately for patients #12, 18, and 32.

G.1 Prediction

G.1.1 Patient #12

We exclude patient #12 from the cohort of the 19 $JAK2^{V617F}$ patients. For the 18 remaining patients, we run a hierarchical Bayesian estimation, as presented in § C.1. For patient #12, we will estimate their parameters, as presented in § C.2, for different assimilation times T. According to the values of T, a different number of VAF measurements are used for the estimation:

- 5 VAF measurements for $T = 300$ days,
- 7 VAF measurements for $T = 600$ days,
- and 10 VAF measurements for $T = 1,000$ days.

In all cases, two measurements of the CF among progenitors are considered, the first at $t = 0$ and the second at $t = 287$ days.

The posterior distributions of the parameters are presented in Fig. G.2, and the results of the predictions are presented in Fig. G.1. The MSE are presented in Tab. G.1. Note that, for $t \geq 1,000$ days, we do not have measurements of the VAF anymore, so we can not compute the prediction error MSE_{pred}^{VAF}.

We get a good agreement between the observed and predicted VAF values already for $T = 300$ days, but we underestimate the values of the homozygous CF. The credibility intervals are large for $T = 300$ days and decrease for $T = 600$ and $T = 1,000$ days.
When looking at the posterior distributions, we can see the impact of the prior knowledge learned from the cohort: the posterior distributions - in particular those of parameters related to heterozygous cells (γ_{het}, $\delta_{0,het}$, ρ_{het}) - are close to the prior distributions, especially for $T = 300$. For η_{het} and η_{hom}, the prior is chosen uniform and, thus, does not come from the cohort. For $\delta_{0,hom}$ and γ_{hom}, their posteriors for $T = 300$ differ from the prior, and we can see how increasing T updates the posteriors. Adding more VAF measurements also seems to impact the estimation of ρ_{hom}; the more data, the less variance we have for the posterior.
However, most of the information comes from the observations before $T = 300$ (and from the prior): the posterior we obtain with $T = 600$ or 1,000 does not differ much from the one we get with $T = 300$. The reason is that, when increasing T, we only add VAF measurements but no additional observations of the CF among progenitors. In general, the posterior distributions of patient #12 are close to the prior, suggesting that their response to the therapy does not deviate too large from those obtained for the 18

	$T = 300$			$T = 600$			$T = 1000$		
	$\mathcal{D}_T^{(i)}$	$\mathcal{D}_c^{(i)}$	$\mathcal{D}^{(i)}$	$\mathcal{D}_T^{(i)}$	$\mathcal{D}_c^{(i)}$	$\mathcal{D}^{(i)}$	$\mathcal{D}_T^{(i)}$	$\mathcal{D}_c^{(i)}$	$\mathcal{D}^{(i)}$
VAF	0.0031	0.0011	0.0021	0.0016	0.0015	0.0015	0.0011	NA	0.001
het CF	0.0087	0.0061	0.0067	0.0108	0.0080	0.0086	0.0111	0.0083	0.0089
hom CF	0.0257	0.0377	0.0353	0.0282	0.0417	0.0390	0.0298	0.0442	0.0414
All	0.0375	0.0449	0.0440	0.0406	0.0512	0.0491	0.0420	NA	0.0514

Table G.1: Results for patient # 12. Values of the MSE computed for different assimilation times T (300, 600, or 1000 days), different types of measurements (VAF among mature cells, heterozygous or homozygous CF among progenitors, or all together), and different observations: either from the control dataset ($\mathcal{D}_c^{(i)}$), the one used for the model calibration ($\mathcal{D}_T^{(i)}$), or the whole dataset ($\mathcal{D}^{(i)}$). For $t \geq 1,000$ days, we do not have measurements of the VAF, so we can not compute the prediction error and displays NA (Not applicable) instead.

remaining patients in the cohort. However, we can also see that there is not a good agreement between the observed and inferred homozygous CF at $t = 287$, suggesting that the dynamics of the VAF would agree with what could be expected for the other patients but not the dynamic of the CF. More broadly, when looking at the residuals, we observe systematic deviations for the heterozygous (overestimation) and homozygous (underestimation) values (most of them being not used for estimating the model parameters). This is in line with the previous comment suggesting that the observed dynamics among progenitor cells for patient # 12 might differ from what would be expected *a priori*. For more reliable predictions concerning the heterozygous and homozygous CF dynamics, more than two measurements of the heterozygous and homozygous CF should be considered when fitting the model.

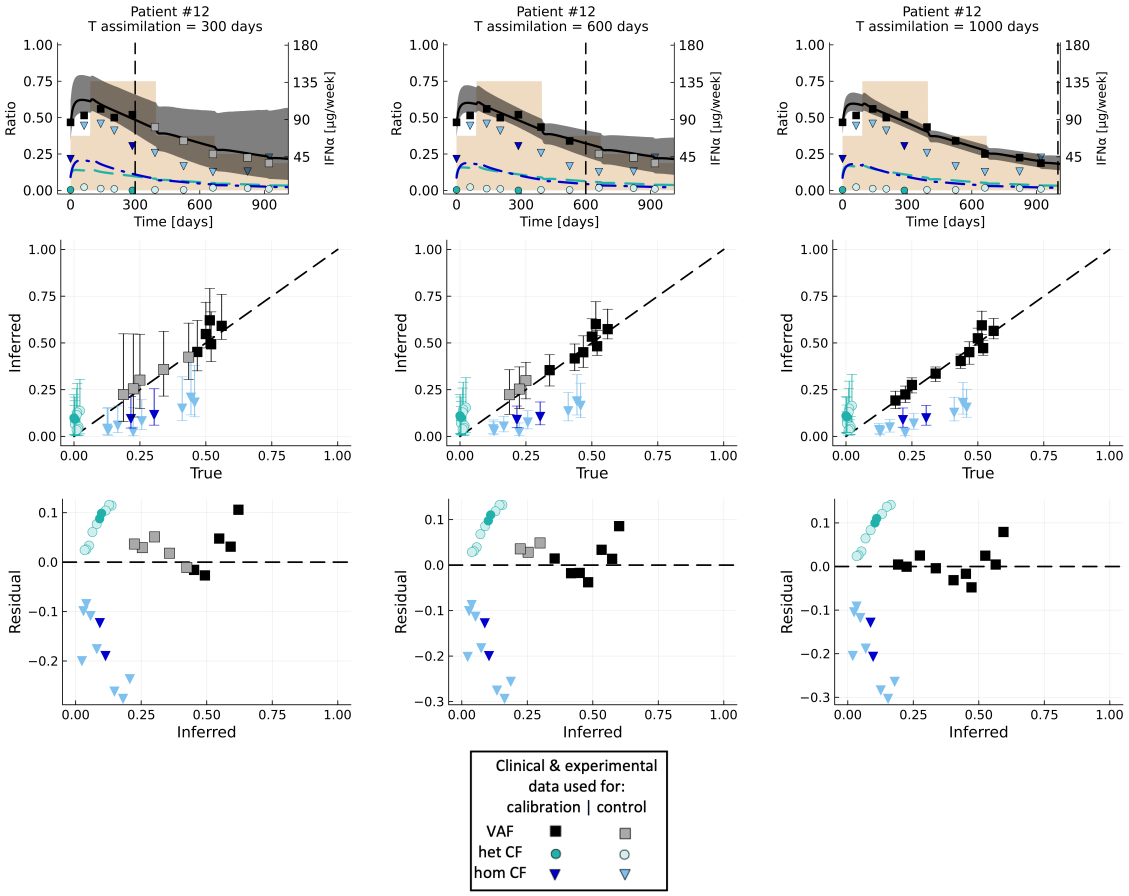

Figure G.1: Data assimilation results for patient #12. From left to right, the assimilation times are $T = 300$, 600, and 1,000 days (vertical dash line). At the top, we present the predicted dynamics. In black, the VAF (median value and 95% credibility interval), and respectively in green and blue, the CF (medians) of heterozygous and homozygous mutated progenitors. The squares, circles, and triangles correspond to the clinical/experimental data, either used to calibrate the model (dark colors), or to control the quality of the predictions (light colors - control dataset). In brown, we represent the IFNα dose variations over treatment (in μg/week).
Second line, we compare the inferred values (median values, in the y-axis) with those observed (in the x-axis) for both the control data set and the one used for the model calibration. The error bars correspond to the 95% credibility intervals. At the bottom, we display the residuals (inferred values minus the observed ones) (y-axis) according to the inferred values (x-axis).

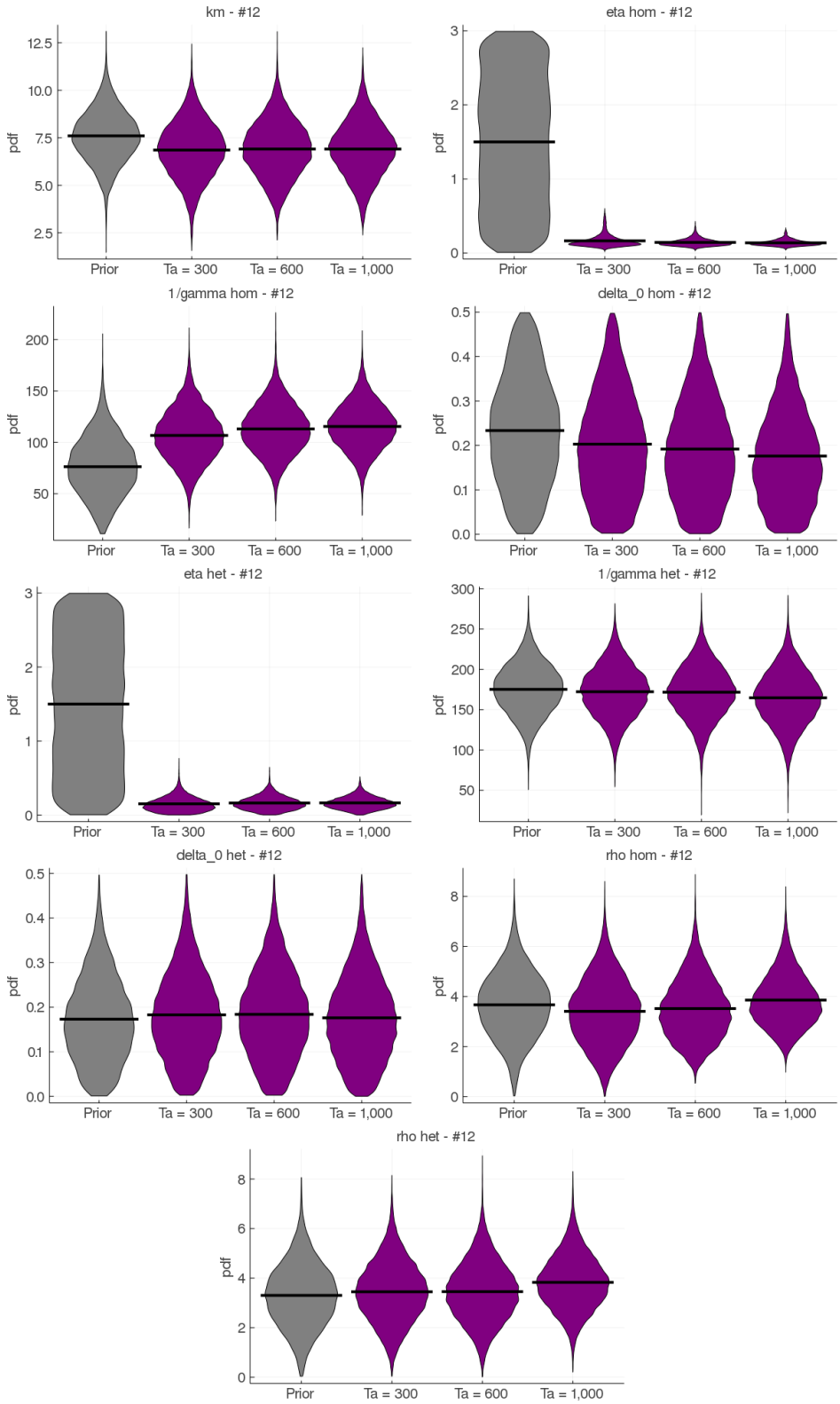

Figure G.2: Posterior distributions (pdf - in purple) of all parameters, for patient #12, according to the assimilation time T. In grey on the left, we display the prior distribution (that is, the one obtained from the hierarchical inference based on the 18 remaining patients). For parameters η_{het} and η_{hom}, which refer to the initial conditions, we choose a non-informative uniform prior. Otherwise, the prior comes from the hierarchical Bayesian estimation made with the data of the 18 remaining patients. The horizontal dark line represents the mean value.

G.1.2 Patient #18

We exclude patient #18 from the cohort of the 19 $JAK2^{V617F}$ patients. For the 18 remaining patients, we run a hierarchical Bayesian estimation, as presented in § C.1. For patient #18, we will estimate their parameters, as presented in § C.2, for different assimilation times T. According to the values of T, a different number of VAF measurements are used for the estimation:

- 4 VAF measurements for $T = 300$ days,
- 8 VAF measurements for $T = 600$ days,
- and 11 VAF measurements for $T = 1,000$ days.

In all cases, two measurements of the CF among progenitors are considered, the first at $t = 0$ and the second at $t = 248$ days.

The parameter posterior distributions are presented in Fig. G.4 and the results of the predictions are presented in Fig. G.3. The MSE are presented in Tab. G.2.
The results for patient #18 were detailed in §3.1 in the main text. In general, we can see a good agreement between the inferred and observed values, both for the VAF and the heterozygous and homozygous CF. We did not observe systematic deviations concerning the observations used for the model calibration. However, we tend to underestimate (for $T = 600$ or $T = 1000$) the predicted values of the homozygous CF when overestimating those of the heterozygous CF, such that there is a compensation leading to a good estimation of the VAF.
For this patient, it is interesting to see how the posterior distribution of some parameters ($\delta_{0,hom}$, $\delta_{0,het}$, ρ_{hom}, γ_{hom}) is updated when adding more and more data (i.e., when increasing the assimilation time T) when for other parameters, the posterior stays close from the prior (k_m, γ_{het}). In particular, the posterior of $\delta_{0,hom}$ largely deviates from the prior, already when $T = 300$, and even more for higher T. It is also interesting to observe that the posterior distributions of η_{het} and η_{hom} - parameters associated with the initial quantities of heterozygous and homozygous mutated cells - remain unchanged when increasing the assimilation time.

	$T = 300$			$T = 600$			$T = 1000$		
	$\mathcal{D}_T^{(i)}$	$\mathcal{D}_c^{(i)}$	$\mathcal{D}^{(i)}$	$\mathcal{D}_T^{(i)}$	$\mathcal{D}_c^{(i)}$	$\mathcal{D}^{(i)}$	$\mathcal{D}_T^{(i)}$	$\mathcal{D}_c^{(i)}$	$\mathcal{D}^{(i)}$
VAF	0.0068	0.0066	0.0067	0.0040	0.0006	0.0026	0.0026	0.0005	0.0021
het CF	0.0002	0.0047	0.0041	0.0016	0.0085	0.0076	0.0027	0.0163	0.0145
hom CF	0.0086	0.0065	0.0068	0.0046	0.0045	0.0045	0.0034	0.0062	0.0058
All	0.0155	0.0177	0.0175	0.0102	0.0136	0.0147	0.0087	0.0231	0.0225

Table G.2: Results for patient # 18. Values of the MSE computed for different assimilation times T (300, 600, or 1000 days), different types of measurements (VAF among mature cells, heterozygous or homozygous CF among progenitors, or all together), and different observations: either from the control dataset ($\mathcal{D}_c^{(i)}$), the one used for the model calibration ($\mathcal{D}_T^{(i)}$), or the whole dataset ($\mathcal{D}^{(i)}$).

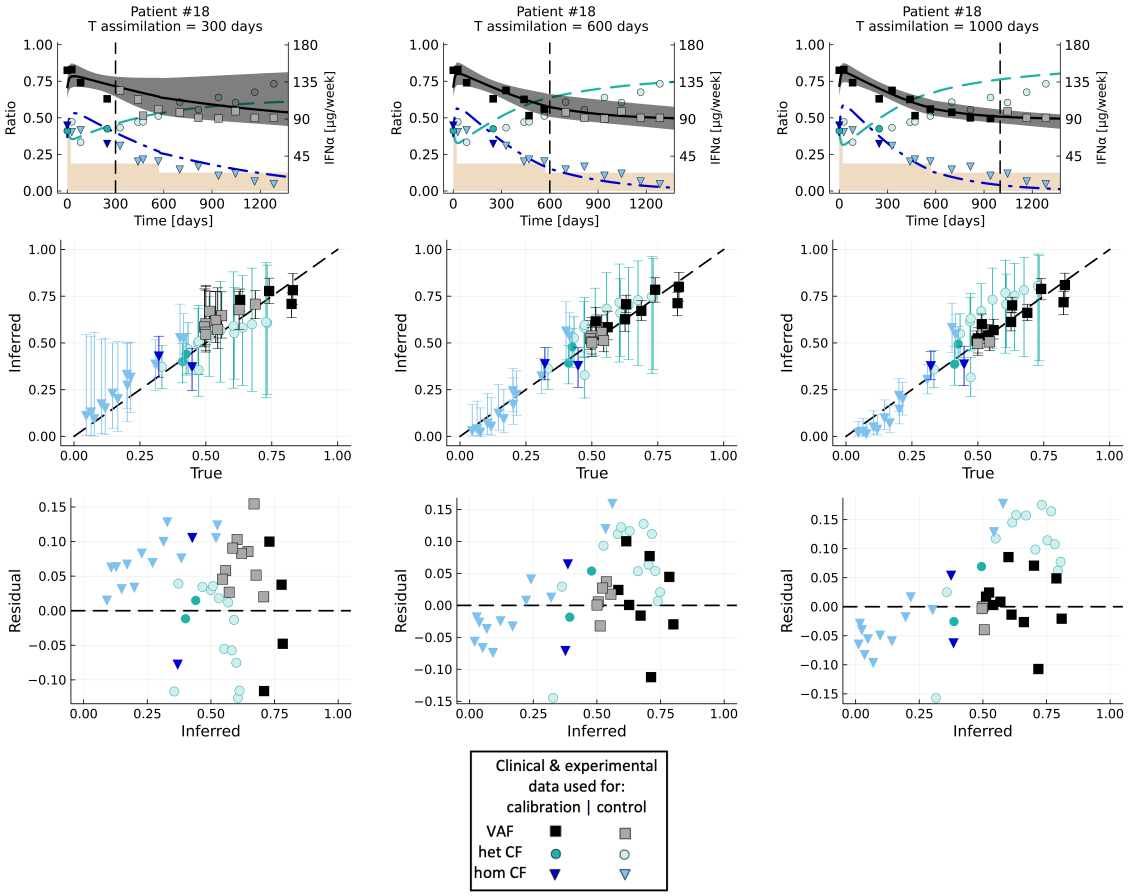

Figure G.3: Data assimilation results for patient #18. From left to right, the assimilation times are $T = 300$, 600, and 1,000 days (vertical dash line). At the top, we present the predicted dynamics. In black, the VAF (median value and 95% credibility interval), and respectively in green and blue, the CF (medians) of heterozygous and homozygous mutated progenitors. The squares, circles, and triangles correspond to the experimental/clinical data, either used to calibrate the model (dark colors), or to control the quality of the predictions (light colors - control dataset). In brown, we represent the IFNα dose variations over treatment (in μg/week).
Second line, we compare the inferred values (median values, in the y-axis) with those observed (in the x-axis) for both the control data set and the one used for the model calibration. The error bars correspond to the 95% credibility intervals. At the bottom, we display the residuals (inferred values minus the observed ones) (y-axis) according to the inferred values (x-axis).

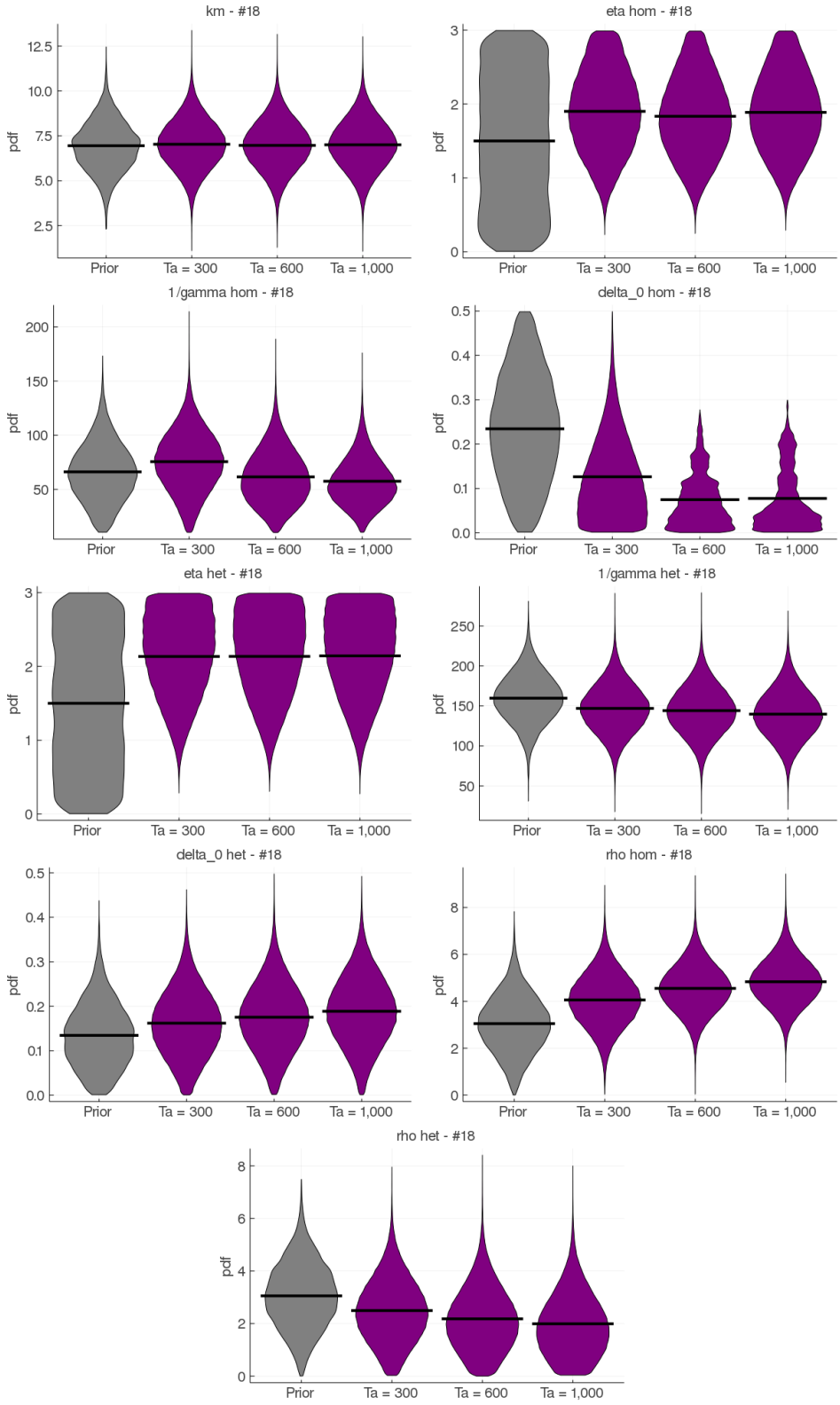

Figure G.4: Posterior distributions (pdf - in purple) of all parameters, for patient #18, according to the assimilation time T. In grey on the left, we display the prior distribution. For parameters η_{het} and η_{hom}, which refer to the initial conditions, we choose a non-informative uniform prior. Otherwise, the prior comes from the hierarchical Bayesian estimation made with the data of the 18 remaining patients. The horizontal dark line represents the mean value.

G.1.3 Patient #32

We exclude patient #32 from the cohort of the 19 $JAK2^{V617F}$ patients. For the 18 remaining patients, we run a hierarchical Bayesian estimation, as presented in § C.1. For patient #32, we will estimate their parameters, as presented in § C.2, for different assimilation times T. According to the values of T, a different number of VAF measurements are used for the estimation:

- 3 VAF measurements for $T = 300$ days,
- 5 VAF measurements for $T = 600$ days,
- and 8 VAF measurements for $T = 1,000$ days.

In all cases, two measurements of the CF among progenitors are considered, the first at $t = 0$ and the second at $t = 235$ days.

The results of the predictions are presented in Fig. G.5. The MSE are presented in Tab. G.3. For $T = 600$, we get poor predictions. Therefore, we study the impact of the choice of another time point for measuring the clonal architecture among progenitors. The results, presented in the next paragraph, show that the poor predictions we get for $T = 600$ can be explained by the choice of the CF used for inferring the dynamics. In other words, the time point for measuring the clonal architecture matters.

	$T = 300$			$T = 600$			$T = 1000$		
	$\mathcal{D}_T^{(i)}$	$\mathcal{D}_c^{(i)}$	$\mathcal{D}^{(i)}$	$\mathcal{D}_T^{(i)}$	$\mathcal{D}_c^{(i)}$	$\mathcal{D}^{(i)}$	$\mathcal{D}_T^{(i)}$	$\mathcal{D}_c^{(i)}$	$\mathcal{D}^{(i)}$
VAF	0.0164	0.0217	0.0205	0.0049	0.2500	0.1557	0.0065	0.0235	0.0130
het CF	0.0022	0.0010	0.0012	0.0033	0.0007	0.0011	0.0012	0.0010	0.0010
hom CF	0.0073	0.0060	0.0062	0.0006	0.0862	0.0730	0.0015	0.0073	0.0064
All	0.0164	0.0287	0.0279	0.0088	0.3370	0.2299	0.0065	0.0318	0.0205

Table G.3: Results for patient # 32. Values of the MSE computed for different assimilation times T (300, 600, or 1000 days), different types of measurements (VAF among mature cells, heterozygous or homozygous CF among progenitors, or all together), and different observations: either from the control dataset ($\mathcal{D}_c^{(i)}$), the one used for the model calibration ($\mathcal{D}_T^{(i)}$), or the whole dataset ($\mathcal{D}^{(i)}$).

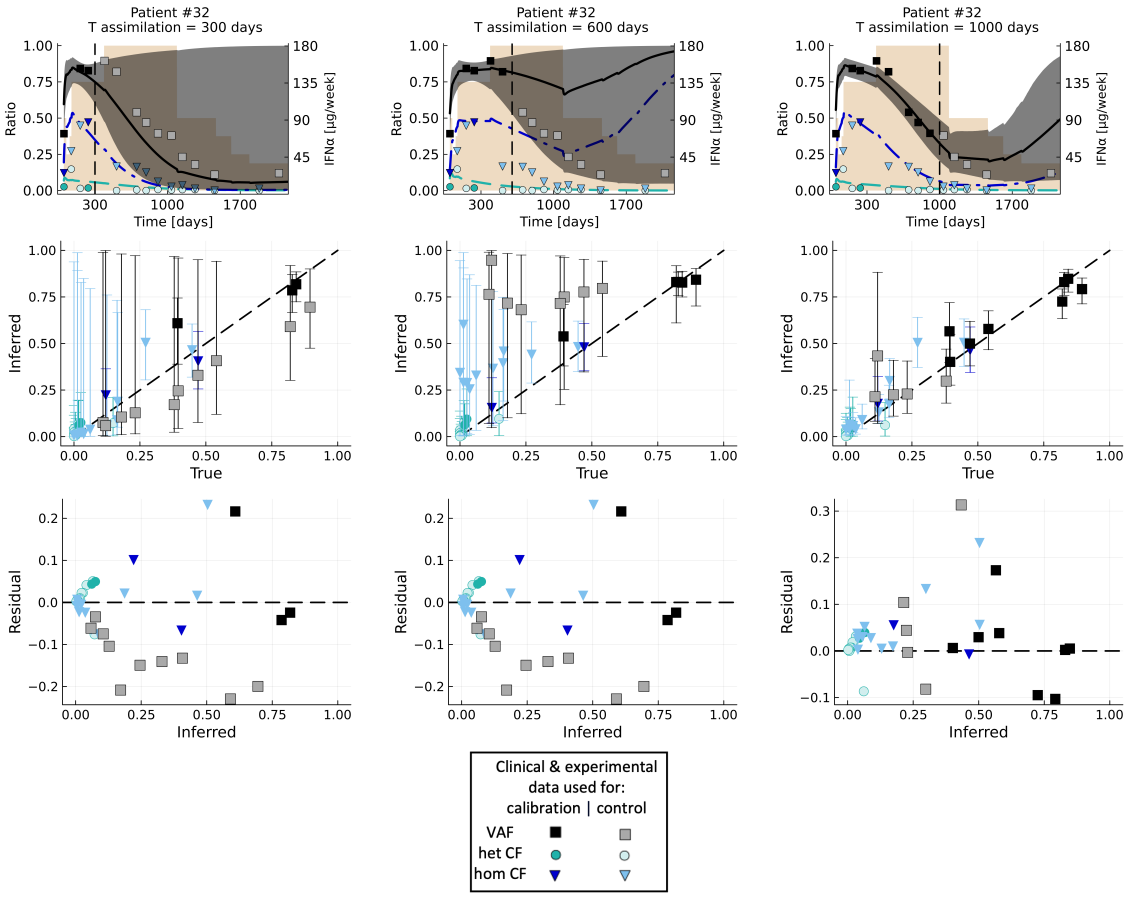

Figure G.5: Data assimilation results for patient #32. From left to right, the assimilation times are $T = 300$, 600, and 1,000 days (vertical dash line). At the top, we present the predicted dynamics. In black, the VAF (median value and 95% credibility interval), and respectively in green and blue, the CF (medians) of heterozygous and homozygous mutated progenitors. The squares, circles, and triangles correspond to the clinical/experimental data, either used to calibrate the model (dark colors), or to control the quality of the predictions (light colors - control dataset). In brown, we represent the IFNα dose variations over treatment (in μg/week).
Second line, we compare the inferred values (median values, in the y-axis) with those observed (in the x-axis) for both the control data set and the one used for the model calibration. The error bars correspond to the 95% credibility intervals. At the bottom, we display the residuals (inferred values minus the observed ones) (y-axis) according to the inferred values (x-axis).

G.1.4 Patient #32 when choosing another time point for measuring the clonal architecture

As we saw in the previous paragraph, the predictions were not good for patient #32 for $T = 600$ and a CF measured at $t = 235$ days. If we run the same computation, but instead of choosing the second CF observation at $t = 235$ days, we consider the one at $t = 508$ days, we obtain the results presented in Fig. G.6. The predictions for $T = 600$ are much better (Tab. G.4), illustrating the importance of the choice of the time point for measuring the clonal architecture. No systematic deviations are observed. When looking at the posterior distributions (Fig. G.7), we can observe that the posterior distributions of the parameters related to heterozygous mutated cells do not deviate from the prior, which is explained by the fact that patient #32 has almost no heterozygous cells. There is especially one parameter - namely ρ_{hom} - whose posterior distribution is updated when increasing the number of VAF measurements.

	$T = 600$			$T = 1000$		
	$\mathcal{D}_T^{(i)}$	$\mathcal{D}_c^{(i)}$	$\mathcal{D}^{(i)}$	$\mathcal{D}_T^{(i)}$	$\mathcal{D}_c^{(i)}$	$\mathcal{D}^{(i)}$
VAF	0.0133	0.0075	0.0097	0.0071	0.0161	0.0106
het CF	0.0006	0.0010	0.0009	0.0004	0.0011	0.0010
hom CF	0.0063	0.0038	0.0042	0.0051	0.0038	0.0040
All	0.0201	0.0123	0.0148	0.0126	0.0210	0.0156

Table G.4: Results for patient # 32, when considering a measurement of the clonal architecture at $t = 0$ and $t = 508$ (Therefore, we do not present the results for $T = 300$). Values of the MSE computed for different assimilation times T (600 or 1000 days), different types of measurements (VAF among mature cells, heterozygous or homozygous CF among progenitors, or all together), and different observations: either from the control dataset ($\mathcal{D}_c^{(i)}$), the one used for the model calibration ($\mathcal{D}_T^{(i)}$), or the whole dataset ($\mathcal{D}^{(i)}$).

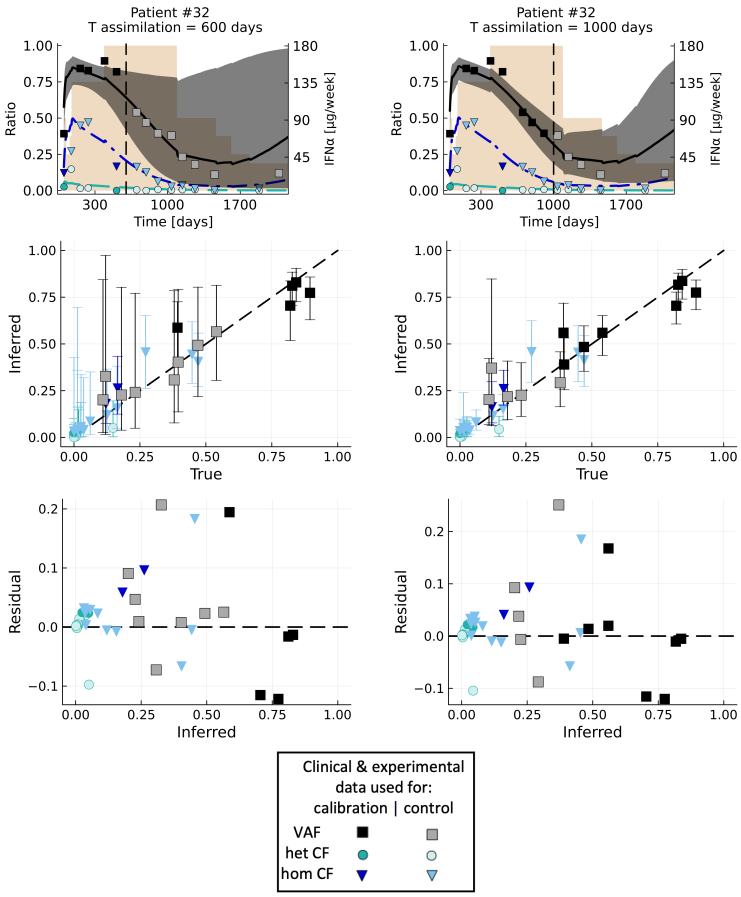

Figure G.6: Data assimilation results for patient #32, when considering a measurement of the clonal architecture at $t = 0$ and $t = 508$ (Therefore, we do not display the results for $T = 300$). On the left, we have $T = 600$, and on the right, $T = 1,000$. At the top, we present the predicted dynamics. In black, the VAF (median value and 95% credibility interval), and respectively in green and blue, the CF (medians) of heterozygous and homozygous mutated progenitors. The squares, circles, and triangles correspond to the clinical/experimental data, either used to calibrate the model (dark colors), or to control the quality of the predictions (light colors - control dataset). In brown, we represent the IFNα dose variations over treatment (in μg/week).
Second line, we compare the inferred values (median values, in the y-axis) with those observed (in the x-axis) for both the control data set and the one used for the model calibration. The error bars correspond to the 95% credibility intervals. At the bottom, we display the residuals (inferred values minus the observed ones) (y-axis) according to the inferred values (x-axis).

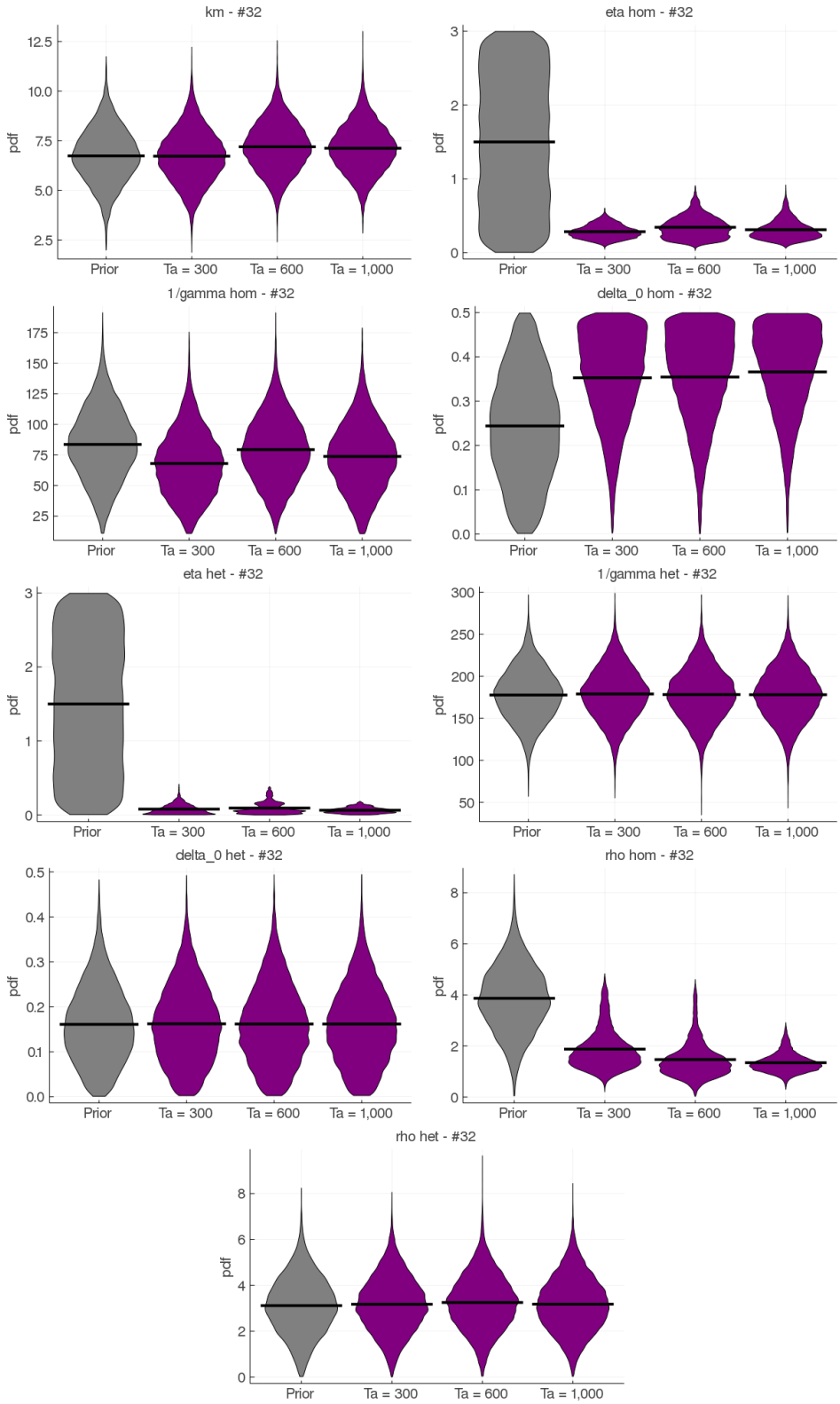

Figure G.7: Posterior distributions (pdf - in purple) of all parameters, for patient #32, according to the assimilation time T. Here, we consider that the CF is measured at $t = 0$ and $t = 508$ (instead of 235). In grey on the left, we display the prior distribution. For parameters η_{het} and η_{hom}, which refer to the initial conditions, we choose a non-informative uniform prior. Otherwise, the prior comes from the hierarchical Bayesian estimation made with the data of the 18 remaining patients. The horizontal dark line represents the mean value.

G.1.5 Synthesis

This section summarises the results we get for patients #12, 18, and 32. In Tab. G.5, we display the predicted error based on the VAF values (MSE_{pred}^{VAF}). In Tab. G.6, we present the estimated parameter vector (mean posterior value) for the assimilation time $T = 600$. These are the values used when studying the treatment optimization (section G.2) and the experimental design (section G.3). The parameter k_m is similar for each of our three patients. It might suggest that the proliferative advantage of the $JAK2^{V617F}$ mutated cells at the last stages of hematopoiesis is a property of the mutated cell and not patient-dependent. η_{het} and η_{hom} correspond to the estimated initial quantities of heterozygous and homozygous mutated HSCs compared to the quantities of WT HSCs. Patient #18 initially has far more mutated cells than the two others, which explains why patient #18 is diagnosed with a PMF, a more advanced disease than PV. The values of $1/\gamma_{het}$ do not much differ between the three patients, and actually, do not differ much from the prior (that is, from the population distribution), suggesting that the effect of IFNα on the quiescence exit of mutated HSCs does not differ much between patients. For homozygous mutated HSCs, on the contrary, the value of $1/\gamma_{hom}$ differs according to the patient, with a trend to have lower values (that is, higher rate of quiescence exit) when there are more mutated HSCs (but three patients is too few to have a statistical significance). Overall, patients # 12 and #18, who have few heterozygous mutated cells, have similar estimated parameter values when associated with heterozygous mutated cells. This is explained by the fact that, for them, the posterior distributions of the parameter associated with the heterozygosity will not differ much from the prior. Patient # 18 will have their heterozygous mutated HSCs slightly less targeted than the two other patients (according to the estimated value for ρ_{het}). However, on the other hand, their homozygous mutated cells will be targeted more efficiently (since patient # 18 has a lower value for $\delta_{0,hom}$ and a higher value for ρ_{hom}, compared to the two others). Here again, the potential difference between patient #18 *vs* patients #12 and 32 might lie in the difference at the beginning of the therapy, that is, a much higher mutated heterozygous and homozygous CF before the start of the treatment.
To sum up, differences between the estimated model parameters could be, of course, explained by an inter-individual heterogeneity, but also by the fact that the patients have different prognostic when they start the therapy, with patient # 18 having the most severe one (PMF) associated with a high proportion of both heterozygous and homozygous mutated cells.

T	#12	#18	#32	#32 (bis)
300	0.0011	0.0066	0.0217	NR
600	0.0015	0.0006	0.2500	0.0075
1,000	NR	0.0005	0.0235	0.0161

Table G.5: Results of the prediction error MSE_{pred}^{VAF}. NR means Not Relevant. #32 (bis) corresponds to the dataset of patient #32 when choosing the second observation for the CF at $t = 508 > 300$.

We also explored the relevance of our observation model - presented in eq. (A.1) - with a QQ-plot in Fig. G.8 or with the residual plots presented at the bottom of Fig. G.1, G.3, G.5, and G.6. However, these results suggest that the assumption of Gaussian distributed errors might not be totally relevant, and other choices could be more appropriate. It should also be recalled that the dynamic model used to describe the on-treatment dynamics of $JAK2^{V617F}$ patients is necessarily a simplification of reality. Consequently, the model could also introduce some biases, explaining why the residuals are not randomly distributed around zero in Fig. G.1, G.3, G.5, and G.6.

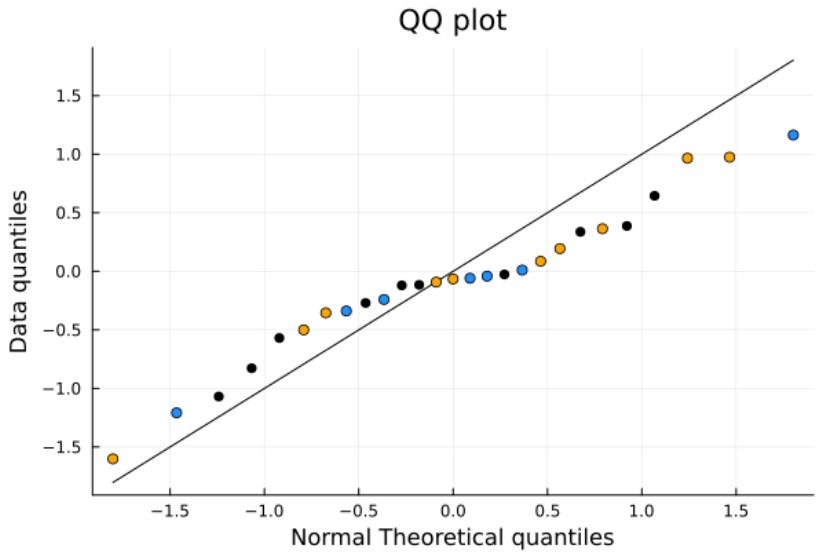

Figure G.8: QQ-plot showing to which extent the assumption of Gaussian distributed errors, as expressed by equation (A.1), holds for the VAF observations (when used to estimate the model parameters). According to equation (A.1), $\hat{y}_k^{(i)} \mid y_k^{(i)} \sim \mathcal{N}\left(y_k^{(i)}, y_k^{(i)}\left(1-y_k^{(i)}\right)\sigma_m^2\right)$, that is, $\frac{\hat{y}_k^{(i)}-y_k^{(i)}}{\sigma_m\sqrt{y_k^{(i)}\left(1-y_k^{(i)}\right)}}$ (y-axis) should be distributed according to a standard Gaussian law (x-axis). Here, $\hat{y}_k^{(i)}$ corresponds to the VAF observed at time $t_k^{(i)}$ for individual i, when $y_k^{(i)}$ corresponds to the theoretical value (median values obtained after propagating the uncertainties from the posterior distribution of the parameters to the model output - computations made with the assimilation time $T = 1,000$ days). The values used for computing the QQ-plot are associated with the VAF measurements obtained before $T = 1,000$ days of treatment for patient #12 (orange circles), #18 (black), and #32 (blue).

The QQ-plot differs from what would be ideally expected if the errors were truly distributed according to eq. (A.1) and if the model was the real one. Our model is necessarily a simplification of reality; it is not excluded that it has some bias and might not be totally suitable to describe the clinical data. However, if not perfect, the considered model resulted from a model selection procedure performed in [9] and therefore turned out to be the most appropriate given a large set of (217) potential models. More likely, the assumption of Gaussian distributed errors, as we initially introduced it in [15], might not be verified, and it would be relevant to explore if some noise models were more suitable.

Parameter	#12	#18	#32 (bis)	Baseline (WT)
k_m	6.97	6.96	7.22	1.0
η_{hom}	0.14	1.83	0.36	-
$1/\gamma_{hom}$	113.0	61.58	80.4	300.0
$\delta_{0,hom}$	0.19	0.07	0.35	0.0
η_{het}	0.16	2.14	0.11	-
$1/\gamma_{het}$	171.8	144.8	178.6	300.0
$\delta_{0,het}$	0.18	0.17	0.16	0.0
ρ_{hom}	3.47	4.55	1.55	0.0
ρ_{het}	3.5	2.18	3.26	0.0
d_{inf}	0.093 (17μg/week)	0.138 (25μg/week)	0.345 (62μg/week)	-

Table G.6: Estimated (mean posterior value) parameter vectors for patient #12, 18, and 32, when the assimilation time is $T = 600$. For patient #32, we present the results when considering a measurement of the CF at time $t = 508 > 300$. In addition, we present the estimated minimal IFNα dose d_{inf} (see § C.2.4). The last column gives an indication of the values we would have for WT cells, or more broadly, for cell populations which, even if mutated, would not have a proliferative advantage compared to WT cells, neither be targeted by IFNα.

G.2 Optimization

For the optimization part of this study, we consider having observed the patient (either patient #12, 18, or 32) before $T = 600$ days. We estimated their parameter vector from the observations before that time, as reported in Tab. G.6. In this section, we aim to optimize the therapy from time $T = 600$ days.

G.2.1 Patient #12

We consider $T = 600$ days. Using the observations of patient #12 before that time (7 VAF observations, two clonal architectures: the first at $t = 0$, the second at $t = 287$ days) and the prior knowledge obtained from the 18 remaining patients, we estimated the posterior distribution of the model parameters previously.
We now consider that the actual parameter vector is the one having been estimated (see Tab. G.6) and study how different dose strategies impact the response to the treatment after $T = 600$ days. With the estimated parameter vector, the minimal dose - under which the treatment would not target sufficiently the mutated HSCs, resulting in a relapse - is estimated to be equal to $d_{inf} = 0.093$, that is, 17μg/week. We consider different scenarios for how drug toxicity increases as a function of the dose, as presented in § 2.3.3 in the main text.
For each scenario, we study our three therapeutic strategies - presented in §2.3.2 in the main text - for which we find the parameters (e.g., the choice of the dose $\bar{d}$) that minimize the value of $M(\tau)$. This latter value corresponds to the toxicity-related amount of IFNα administered from T to the time τ, this latter being the time when the therapy could be interrupted (section D). We can compare the three therapeutic strategies for a given drug-toxicity relation and select the one with the best (i.e., the lowest) value for $M(\tau)$. Results are presented in Fig. G.9. It turns out that the constant strategy is found to be the most optimal for the linear and the concave scenario. For the convex scenario, the parameter vectors which minimize $M(\tau)$ for the periodic and the decreasing strategies are such that the three optimal strategies are almost the same. For the composite relation, $d_{inf} = 0.093 < d_{low} := 0.1$, d_{low} being the threshold below which we consider there is no toxicity (see E.4). Thus, it turns out in that case that each therapeutic strategy can be optimized to avoid administrating a dose above the value of d_{low}, such that we end up with a zero value for $M(\tau)$. Under the hypothesis of the composite dose-toxicity relation, all optimal therapeutic strategies are close to the constant one. Thus, the constant strategy can also here be considered the most optimal.

For patient #12, the trade-off would be to treat them with a decreasing dose, starting at $T = 600$ days with $\bar{d} = 86\mu$g/week, a decreasing factor $\lambda = 0.45$, and a period $L = 16$ months, until the treatment could be interrupted, here at age 77. This trade-off strategy would be:

- in the top 22 percent if the dose-toxicity relation were linear,
- in the top 46 percent if the dose-toxicity relation were convex,
- in the top 46 percent if the dose-toxicity relation were concave,
- and in the top 47 percent if the dose-toxicity relation were composite.

G.2.2 Patient #18

Using the observations of patient #18 before $T = 600$ (8 VAF observations, two clonal architectures: the first at $t = 0$, the second at $t = 248$ days) and the prior knowledge obtained from the 18 remaining patients, we previously estimated the posterior distribution of the model parameters.
We now consider that the actual parameter vector is the estimated one (see Tab. G.6) and study how different dose strategies impact the response of the treatment after $T = 600$ days. With the estimated parameter vector, the minimal dose is estimated to be equal to $d_{inf} = 0.138$, that is, 25μg/week.
The constant strategy is found to be the most optimal for each of the four scenarios of dose-toxicity we study (Fig. G.10).

For patient #18, the trade-off would be to treat them with a constant dose of 61μg/week, until the treatment could be interrupted, here at age 72. This trade-off strategy would be:

- in the top 0.09 percent if the dose-toxicity relation were linear,
- in the top 6.6 percent if the dose-toxicity relation were convex,
- in the top 7.5 percent if the dose-toxicity relation were concave,
- and in the top 3.9 percent if the dose-toxicity were composite.

G.2.3 Patient #32

The results related to patient #32 have been detailed in the main text (§3.2). Results are also displayed here in Fig. G.11.

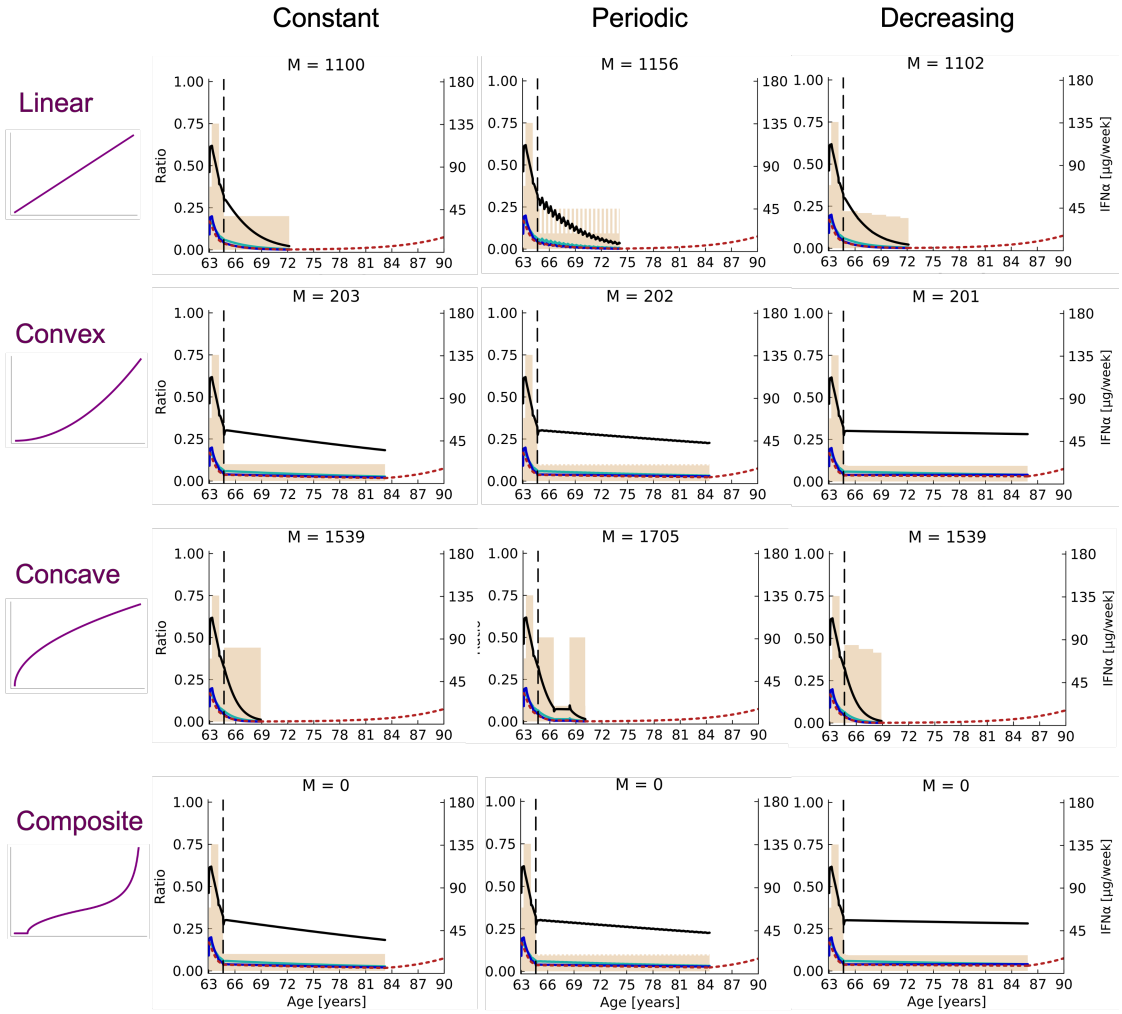

Figure G.9: Results of the treatment optimization for patient #12. Four hypothetical relationships between IFNα toxicity and the dose are studied: linear (at the top), convex (second line), concave (third line), and composite (at the bottom). For each of them, three therapeutic strategies - constant on the left, periodic on the middle, and decreasing on the right - are optimized to minimize $M(\tau)$ (denoted by M on the figures), which is the toxicity-related amount of IFNα administered from T (vertical dashed line) to the treatment interruption time τ (when the weekly dose of interferon - represented in beige - drops to zero). The dynamics of the VAF among mature cells (black line), the heterozygous CF among progenitors (green line), the homozygous CF among progenitors (blue line), and the VAF among HSCs (red dotted line) will differ for $t \geq T$ according to how the doses vary (depending on the considered therapeutic strategy and its parameter values). After the treatment interruption, only the dynamics of the VAF among HSCs is computed (and displayed), according to equation (D.3). All graphs are displayed until 90 years old, the age above which the VAF among HSCs should not exceed 7.5%, as explained in section D. M values are only comparable for a given dose-toxicity relation; the lower, the better.

If the actual dose-toxicity relation were linear, the constant strategy would be optimal for $\bar{d} = 36\mu$g/week (with the associated age of treatment interruption $\tau = 72$ years and an optimal value of $M(\tau) = 1101$), the periodic strategy would be optimal for $\bar{d} = 43\mu$g/week and $L = 3$ months, and the decreasing one for $\bar{d} = 40\mu$g/week, $L = 20$ months, and $\lambda = 0.95$. Among these three strategies, the constant one is the best.

If the actual dose-toxicity relation were convex, the constant strategy would be optimal for $\bar{d} = 18\mu$g/week, the periodic strategy would be optimal for $\bar{d} = 18\mu$g/week and $L = 3$ months, and the decreasing one for $\bar{d} = 18\mu$g/week, $L = 3$ months, and $\lambda = 0.95$.

If the actual dose-toxicity relation were concave, the constant strategy would be optimal for $\bar{d} = 79\mu$g/week, the periodic strategy would be optimal for $\bar{d} = 90\mu$g/week and $L = 22$ months, and the decreasing one for $\bar{d} = 83\mu$g/week, $L = 18$ months, and $\lambda = 0.95$. Among these three strategies, the constant and decreasing ones are both the best.

If the actual dose-toxicity were composite, with a low threshold $d_{low} = 0.1$ below which zero toxicity is assumed, then each strategy for which the dose is maintained below this threshold would lead to a zero value for $M(\tau)$.

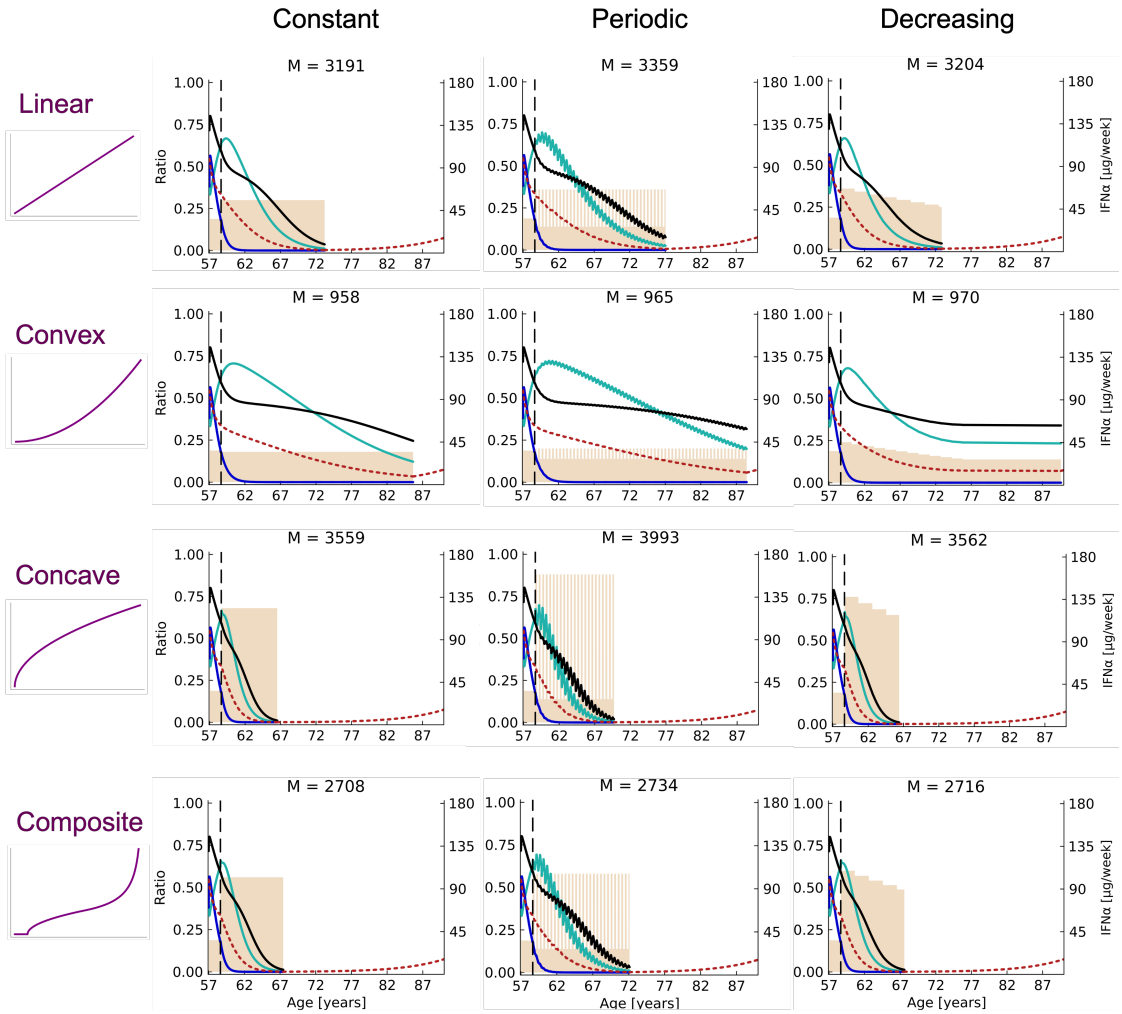

Figure G.10: Results of the treatment optimization for patient #18. Four hypothetical relationships between IFNα toxicity and the dose are studied: linear (at the top), convex (second line), concave (third line), and composite (at the bottom). For each of them, three therapeutic strategies - constant on the left, periodic on the middle, and decreasing on the right - are optimized to minimize $M(\tau)$ (denoted by M on the figures), which is the toxicity-related amount of IFNα administered from T (vertical dashed line) to the treatment interruption time τ (when the weekly dose of interferon - represented in beige - drops to zero). The dynamics of the VAF among mature cells (black line), the heterozygous CF among progenitors (green line), the homozygous CF among progenitors (blue line), and the VAF among HSCs (red dotted line) will differ for $t \geq T$ according to how the doses vary (depending on the considered therapeutic strategy and its parameter values). After the treatment interruption, only the dynamics of the VAF among HSCs is computed (and displayed), according to equation (D.3). All graphs are displayed until 90 years old, the age above which the VAF among HSCs should not exceed 7.5%, as explained in section D. M values are only comparable for a given dose-toxicity relation; the lower, the better.

If the actual dose-toxicity relation were linear, the constant strategy would be optimal for $\bar{d} = 54\mu$g/week (with the associated age of treatment interruption $\tau = 73$ years and an optimal value of $M(\tau) = 3191$), the periodic strategy would be optimal for $\bar{d} = 65\mu$g/week and $L = 3$ months, and the decreasing one for $\bar{d} = 65\mu$g/week, $L = 2$ years, and $\lambda = 0.95$. Among these three strategies, the constant one is the best.

If the actual dose-toxicity relation were convex, the constant strategy would be optimal for $\bar{d} = 32\mu$g/week, the periodic strategy would be optimal for $\bar{d} = 36\mu$g/week and $L = 3$ months, and the decreasing one for $\bar{d} = 43\mu$g/week, $L = 19$ months, and $\lambda = 0.95$.

If the actual dose-toxicity relation were concave, the constant strategy would be optimal for $\bar{d} = 122\mu$g/week, the periodic strategy would be optimal for $\bar{d} = 157\mu$g/week and $L = 3$ months, and the decreasing one for $\bar{d} = 137\mu$g/week, $L = 2$ years, and $\lambda = 0.95$. Among these three strategies, the constant one is the best.

If the actual dose-toxicity relation were composite, the constant strategy would be optimal for $\bar{d} = 100\mu$g/week, the periodic strategy would be optimal for $\bar{d} = 104\mu$g/week and $L = 3$ months, and the decreasing one for $\bar{d} = 108\mu$g/week, $L = 2$ years, and $\lambda = 0.95$. Among these three strategies, the constant one is the best.

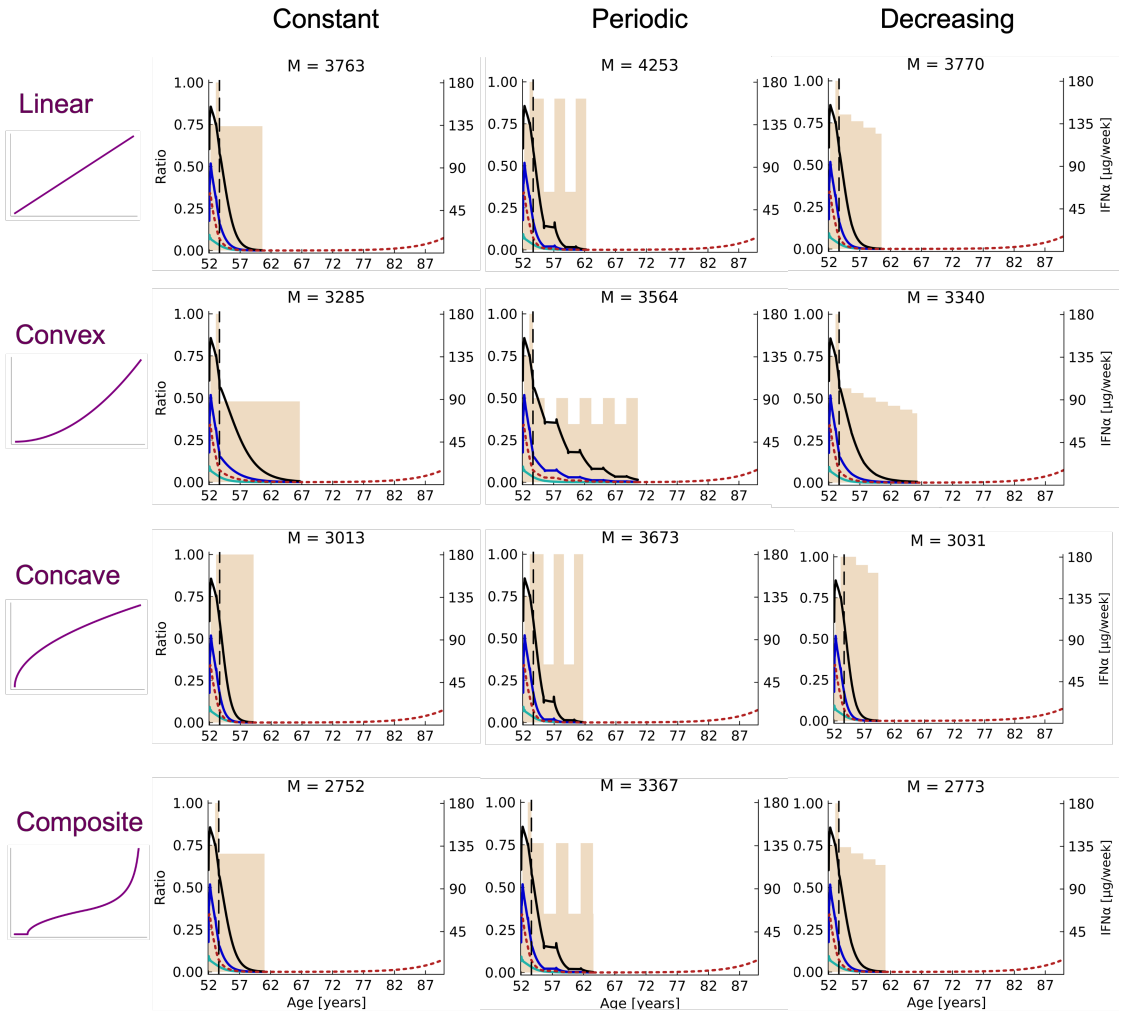

Figure G.11: Results of the treatment optimization for patient #32. Four hypothetical relationships between IFNα toxicity and the dose are studied: linear (at the top), convex (second line), concave (third line), and composite (at the bottom). For each of them, three therapeutic strategies - constant on the left, periodic on the middle, and decreasing on the right - are optimized to minimize $M(\tau)$ (denoted by M on the figures), which is the toxicity-related amount of IFNα administered from T (vertical dashed line) to the treatment interruption time τ (when the weekly dose of interferon - represented in beige - drops to zero). The dynamics of the VAF among mature cells (black line), the heterozygous CF among progenitors (green line), the homozygous CF among progenitors (blue line), and the VAF among HSCs (red dotted line) will differ for $t \geq T$ according to how the doses vary (depending on the considered therapeutic strategy and its parameter values). After the treatment interruption, only the dynamics of the VAF among HSCs is computed (and displayed), according to equation (D.3). All graphs are displayed until 90 years old, the age above which the VAF among HSCs should not exceed 7.5%, as explained in §D. M values are only comparable for a given dose-toxicity relation; the lower, the better.

If the actual dose-toxicity relation were linear, the constant strategy would be optimal for $\bar{d} = 135\mu$g/week (with the associated age of treatment interruption $\tau = 61$ years and an optimal value of $M(\tau) = 3764$), the periodic strategy would be optimal for $\bar{d} = 153\mu$g/week and $L = 22$ months, and the decreasing one for $\bar{d} = 144\mu$g/week, $L = 2$ years, and $\lambda = 0.95$. Among these three strategies, the constant one is the best.

If the actual dose-toxicity relation were convex, the constant strategy would be optimal for $\bar{d} = 86\mu$g/week, the periodic strategy would be optimal for $\bar{d} = 90\mu$g/week and $L = 23$ months, and the decreasing one for $\bar{d} = 100\mu$g/week, $L = 2$ years, and $\lambda = 0.95$. Among these three strategies, the constant one is the best.

If the actual dose-toxicity relation were concave, the constant strategy would be optimal for $\bar{d} = 180\mu$g/week, the periodic strategy would be optimal for $\bar{d} = 180\mu$g/week and $L = 20$ months, and the decreasing one for $\bar{d} = 180\mu$g/week, $L = 2$ years, and $\lambda = 0.95$. Among these three strategies, the constant one is the best.

If the actual dose-toxicity relation were composite, the constant strategy would be optimal for $\bar{d} = 126\mu$g/week, the periodic strategy would be optimal for $\bar{d} = 137\mu$g/week and $L = 2$ years, and the decreasing one for $\bar{d} = 133\mu$g/week, $L = 2$ years, and $\lambda = 0.95$. Among these three strategies, the constant one is the best.

G.3 Experimental Design

Our capacity to recommend good therapeutic strategies to clinicians depends on our capacity to correctly infer the model parameters of new patients, from only minimal observations. We showed in section G.1 that two observations of the clonal architecture and several VAF measurements before 600 days were sufficient to get accurate predictions. But we also illustrated with patient #32 that the quality of the predictions could highly depend on when the clonal architecture is measured (Section G.1.4). In this section, we aim to investigate whether the choice of the timing for measuring the heterozygous and homozygous CF could be rationalized. We apply the method we described in section F, and present first the results we get for patient #12, then the results for patients #18 and #32.

We consider $T = 600$ days. Using the clinical observations of patient #12 before that time (7 VAF observations, two clonal architectures: one at $t = 0$, the second one at $t = 287$) and the prior knowledge obtained from the 18 remaining patients, we estimated the posterior distribution of the model parameters and showed that we could make good predictions (section G.1.1).
We now consider that the actual parameter vector is the one having been estimated (mean of the posterior distribution). From it, we get the theoretical dynamics of the VAF and the heterozygous and homozygous CF over $[0, 600]$ days (solid lines on the top of Fig. G.12). We simulate 600 different synthetic datasets $\mathcal{D}_{T_{obs}}$. All of them have in common 7 VAF values (pseudo-observations) - obtained from the theoretical values by adding some noise - and the CF (pseudo-observation) at the initial time. All of them differ in the time point T_{obs} of the second CF (pseudo-observation). For each value of $T_{obs} \in \{1, 2, \cdots, 600\}$, we estimate the parameter vector that maximizes the posterior density function, and infer the associated CF dynamics. We can then evaluate the error between the estimated and the theoretical CF dynamics, and find for which T_{obs} the error is minimal. Results for patient #12 are presented in Fig. G.12. For them, we find that the pseudo-observation time that would result in the most accurate parameter estimation is $T_{obs} = 100$ days, that is, about three months after the start of the therapy. This observation time corresponds to when the theoretical VAF and CF for patient #12 are maximal over $[0, 600]$, and also when there is a dose increase. However, when applying the same methods with patients #18 and #32, we find that it would be better to observe the clonal architecture later, at 476 days after the start of the therapy for patient #18 (Fig. G.13), when, for patient #32, the error between the theoretical and inferred CF is continuously decreasing when increasing the pseudo-observation time (Fig. G.14.) We are therefore unable to identify a common trend from the study of these three patients and only show that there would be better timings than others, which would be potentially patient-dependent.

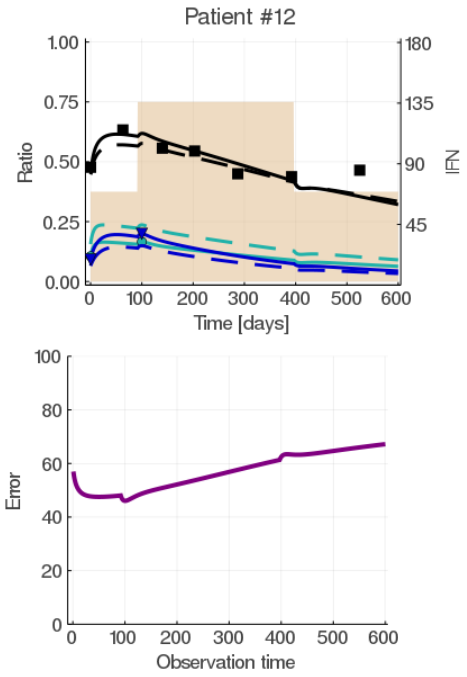

Figure G.12: Optimal experimental design for patient #12. From the theoretical VAF dynamics (solid black line) of patient #12, we simulate noisy VAF pseudo-observations (black square). From the theoretical dynamics of the heterozygous (solid green line) and homozygous (solid blue line), we consider that we observe (pseudo-observations) the CF at the initial time and also at an additional observation time T_{obs}. In the bottom (purple line), we show the error between the theoretical and the inferred CF (L1-norm) according to the choice of T_{obs}. We see that the error would be minimal for $T_{obs} = 100$. On the top, the dashed lines correspond to the inferred dynamics when the synthetic dataset includes the CF pseudo-observation at $T_{obs} = 100$ days.

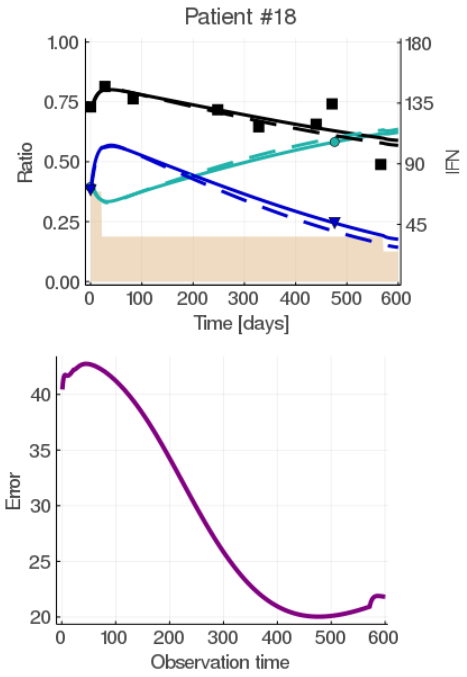

Figure G.13: Optimal experimental design for patient #18. From the theoretical VAF dynamics (solid black line) of patient #18, we simulate noisy VAF pseudo-observations (black square). From the theoretical dynamics of the heterozygous (solid green line) and homozygous (solid blue line), we consider that we observe the CF (pseudo-observations) at the initial time and also at an additional observation time T_{obs}. In the bottom (purple line), we show the error between the theoretical and the inferred CF (L1-norm) according to the choice of T_{obs}. We see that the error would be minimal for $T_{obs} = 476$. On the top, the dashed lines correspond to the inferred dynamics when the simulated dataset includes the CF pseudo-observation at $T_{obs} = 476$ days.

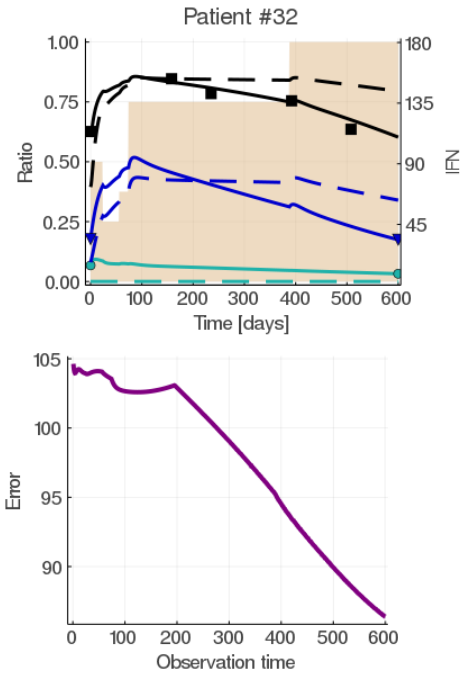

Figure G.14: Optimal experimental design for patient #32. From the theoretical VAF dynamics (solid black line) of patient #32, we simulate noisy VAF pseudo-observations (black square). From the theoretical dynamics of the heterozygous (solid green line) and homozygous (solid blue line), we consider that we observe (pseudo-observations) the CF at the initial time and also at an additional observation time T_{obs}. In the bottom (purple line), we show the error between the theoretical and the inferred CF (L1-norm) according to the choice of T_{obs}. We see that the error continuously decreases with T_{obs}. On the top, the dashed lines correspond to the inferred dynamics when the simulated dataset includes the CF pseudo-observation at $T_{obs} = 600$ days.

References

[1] Catlin, S. N., Abkowitz, J. L., and Guttorp, P. Statistical inference in a two-compartment model for hematopoiesis. *Biometrics 57*, 2 (2001), 546–553.

[2] Dupont, S., Massé, A., James, C., Teyssandier, I., Lécluse, Y., Larbret, F., Ugo, V., Saulnier, P., Koscielny, S., Le Couédic, J. P., et al. The jak2 617v¿ f mutation triggers erythropoietin hypersensitivity and terminal erythroid amplification in primary cells from patients with polycythemia vera. *Blood, The Journal of the American Society of Hematology 110*, 3 (2007), 1013–1021.

[3] Geman, S., and Geman, D. Stochastic relaxation, gibbs distributions, and the bayesian restoration of images. *IEEE Transactions on pattern analysis and machine intelligence*, 6 (1984), 721–741.

[4] Hansen, N. The cma evolution strategy: a comparing review. *Towards a new evolutionary computation* (2006), 75–102.

[5] Hansen, N. The cma evolution strategy: A tutorial. *arXiv preprint arXiv:1604.00772* (2016).

[6] Hasan, S., Lacout, C., Marty, C., Cuingnet, M., Solary, E., Vainchenker, W., and Villeval, J.-L. Jak2v617f expression in mice amplifies early hematopoietic cells and gives them a competitive advantage that is hampered by ifnα. *Blood, The Journal of the American Society of Hematology 122*, 8 (2013), 1464–1477.

[7] Hastings, W. K. Monte carlo sampling methods using markov chains and their applications.

[8] Hermange, G., Rakotonirainy, A., Bentriou, M., Tisserand, A., El-Khoury, M., Girodon, F., Marzac, C., Vainchenker, W., Plo, I., and Cournède, P.-H. Inferring the initiation and development of myeloproliferative neoplasms. *Proceedings of the National Academy of Sciences 119*, 37 (2022), e2120374119.

[9] Hermange, G., Vainchenker, W., Plo, I., and Cournède, P.-H. Mathematical modelling, selection and hierarchical inference to determine the minimal dose in ifnα therapy against myeloproliferative neoplasms. *arXiv preprint arXiv:2112.10688* (2021).

[10] Kiladjian, J.-J. Final results of ruxopeg, a phase 1/2 adaptive randomized trial of ruxolitinib (rux) and pegylated interferon alpha (ifna) 2a in patients with myelofibrosis (mf). In *64th ASH Annual Meeting and Exposition* (2022), ASH.

[11] Kontis, V., Bennett, J. E., Mathers, C. D., Li, G., Foreman, K., and Ezzati, M. Future life expectancy in 35 industrialised countries: projections with a bayesian model ensemble. *The Lancet 389*, 10076 (2017), 1323–1335.

[12] Lee-Six, H., Øbro, N. F., Shepherd, M. S., Grossmann, S., Dawson, K., Belmonte, M., Osborne, R. J., Huntly, B. J., Martincorena, I., Anderson, E., et al. Population dynamics of normal human blood inferred from somatic mutations. *Nature 561*, 7724 (2018), 473–478.

[13] Mann, H. B., and Whitney, D. R. On a test of whether one of two random variables is stochastically larger than the other. *The annals of mathematical statistics* (1947), 50–60.

[14] Michor, F., Hughes, T. P., Iwasa, Y., Branford, S., Shah, N. P., Sawyers, C. L., and Nowak, M. A. Dynamics of chronic myeloid leukaemia. *Nature 435*, 7046 (2005), 1267–1270.

[15] Mosca, M., Hermange, G., Tisserand, A., Noble, R., Marzac, C., Marty, C., Le Sueur, C., Campario, H., Vertenoeil, G., El-Khoury, M., et al. Inferring the dynamics of mutated hematopoietic stem and progenitor cells induced by ifnα in myeloproliferative neoplasms. *Blood* (2021).

[16] Van Egeren, D., Escabi, J., Nguyen, M., Liu, S., Reilly, C. R., Patel, S., Kamaz, B., Kalyva, M., DeAngelo, D. J., Galinsky, I., et al. Reconstructing the lineage histories and differentiation trajectories of individual cancer cells in myeloproliferative neoplasms. *Cell stem cell 28*, 3 (2021), 514–523.

[17] Williams, N., Lee, J., Mitchell, E., Moore, L., Baxter, E. J., Hewinson, J., Dawson, K. J., Menzies, A., Godfrey, A. L., Green, A. R., et al. Life histories of myeloproliferative neoplasms inferred from phylogenies. *Nature 602*, 7895 (2022), 162–168.